

# **The Contributions to the Explosive Growth of PM<sub>2.5</sub> Mass due to Aerosols-Radiation Feedback and Further Decrease in Turbulent Diffusion during a Red-alert Heavy Haze in Jing-Jin-Ji in China**

Hong Wang<sup>1,2\*</sup>, Yue Peng<sup>1,2</sup>, Xiaoye Zhang<sup>1,3\*</sup>, Hongli Liu<sup>1</sup>, Meng Zhang<sup>4</sup>, Huizheng Che<sup>1</sup>, Yanli Cheng<sup>1</sup>, Yu Zheng<sup>1,2</sup>

Author list:

Hong Wang, [wangh@cma.gov.cn](mailto:wangh@cma.gov.cn),

Yue Peng, [1131509950@qq.com](mailto:1131509950@qq.com); [nuist PY@163.com](mailto:nuist_PY@163.com)

Xiaoye Zhang, [xiaoye@cma.gov.cn](mailto:xiaoye@cma.gov.cn)

Hongli Liu, [liuhl@cma.gov.cn](mailto:liuhl@cma.gov.cn)

Meng Zhang, [316398453@qq.com](mailto:316398453@qq.com)

Huizheng Che, [chehz@cma.gov.cn](mailto:chehz@cma.gov.cn)

Yanli Cheng, [chengyl@cma.gov.cn](mailto:chengyl@cma.gov.cn)

Yu Zheng, [hblfzhengyu@126.com](mailto:hblfzhengyu@126.com)

1 **The Contributions to the Explosive Growth of PM<sub>2.5</sub> Mass due**  
2 **to Aerosols-Radiation Feedback and Further Decrease in**  
3 **Turbulent Diffusion during a Red-alert Heavy Haze in**  
4 **Jing-Jin-Ji in China**

5 Hong Wang<sup>1,2\*</sup>, Yue Peng<sup>1,2</sup>, Xiaoye Zhang<sup>1,3\*</sup>, Hongli Liu<sup>1</sup>, Meng Zhang<sup>4</sup>, Huizheng  
6 Che<sup>1</sup>, Yanli Cheng<sup>1</sup>, Yu Zheng<sup>1,2</sup>

7 <sup>1</sup> State Key Laboratory of Severe Weather (LASW), Chinese Academy of Meteorological Sciences (CAMS), CMA, Beijing 100081, China

8 <sup>2</sup> Collaborative Innovation Center on Forecast and Evaluation of Meteorological Disasters, Nanjing University of Information Science & Technology, Nanjing  
9 210044, China

10 <sup>3</sup> Center for Excellence in Regional Atmospheric Environment, Institute of Urban Environment, Chinese Academy of Sciences (CAS), Xiamen 361021, China

11 <sup>4</sup> Beijing Meteorological Bureau, Beijing 100089, China

12 Correspondence to: Hong Wang (wangh@cma.gov.cn), Xiaoye Zhang (xiaoye@cma.gov.cn)

13

14

15 **Abstract.** The explosive growth of PM<sub>2.5</sub> mass usually results in extreme PM<sub>2.5</sub> levels and severe haze  
16 pollution in East China, and is generally underestimated by current atmospheric chemistry models. Based  
17 on one such model, GRPAES\_CUACE, three sensitivity experiments – a “background” experiment (EXP1),  
18 “online aerosol feedback” experiment (EXP2), and an “80% decrease in turbulent diffusion coefficient”  
19 (DTD) of chemical tracers” experiment, based on EXP2 (EXP3) – were designed to study the contributions  
20 of aerosol–radiation feedback (AF) and DTD to the explosive growth of PM<sub>2.5</sub> during a “red-alert” heavy  
21 haze event in China’s Jing–Jin–Ji region. The results showed that the turbulent diffusion coefficient (DC)  
22 calculated by EXP1 was about 60–70 m<sup>2</sup>/s on the clear day and 30–35 m<sup>2</sup>/s on the haze day. This difference  
23 in DC was not enough to distinguish between the unstable atmosphere on the clear day and extremely  
24 stable atmosphere during the PM<sub>2.5</sub> explosive growth stage. Also, the inversion calculated by EXP1 was  
25 obviously weaker than the actual inversion from sounding observations on the haze day. This led to a 40%–  
26 51% underestimation of PM<sub>2.5</sub> by EXP1; AF reduced by about 43%–57% DC during the PM<sub>2.5</sub> explosive  
27 growth stage, which strengthened the local inversion obviously; plus, the local inversion indicated by EXP2  
28 was much closer to the sounding observations than that by EXP1. This resulted in a 20%–25% reduction of

29  $PM_{2.5}$  negative errors in the model, reaching as low as  $-16\%$  to  $-11\%$  in EXP2. However, the inversion  
30 produced by EXP2 was still weaker than the actual observation, and AF could not solve all the problems of  
31  $PM_{2.5}$  underestimation. Based on EXP2, the 80% DTD of chemical tracers in EXP3 resulted in near-zero  
32 turbulent diffusion, referred to as an “turbulent intermittence” atmospheric state, which resulted in a further  
33 14%–20% reduction in  $PM_{2.5}$  underestimation, and the negative  $PM_{2.5}$  errors were reduced to  $-11\%$  to 2%.  
34 The combined effects of AF and DTD solved over 79% of the underestimation of the explosive growth of  
35  $PM_{2.5}$  in this study. The results show that online calculation of AF is essential for the prediction of  $PM_{2.5}$   
36 explosive growth and peaks during severe haze in China’s Jing–Jin–Ji region. Besides, an improving in the  
37 planetary boundary layer scheme with respect to extremely stable atmospheric stratification is also essential  
38 for a reasonable description of local “turbulent intermittence” and a more accurate prediction of  $PM_{2.5}$   
39 explosive growth during severe haze in in this region of China.  
40 **Keywords:** aerosol–radiation feedback; turbulent diffusion; planetary boundary layer scheme; temperature  
41 inversion;  $PM_{2.5}$

## 42 **1 Introduction**

43 Since 2013, East China has been experiencing unprecedented intrusions of severe haze accompanied  
44 by high levels of particulate matter (PM) of less than 2.5 microns in aerodynamic diameter ( $PM_{2.5}$ ), causing  
45 wide public concern (Ding et al., 2013; Wang et al. 2013; Huang et al., 2014; Wang et al., 2014; Sun et al.,  
46 2014; Hua et al., 2016; Yang et al., 2015; Zhong et al., 2017, 2018a, 2018b). The instantaneous  $PM_{2.5}$   
47 concentration is usually in the hundreds of  $ug/m^3$  during severe haze episodes, occasionally exceeding one  
48 thousand, in the metropolitan region of Beijing–Tianjin–Hebei, referred to here as Jing–Jin–Ji, and its  
49 surroundings of East Shanxi, West Shandong, and North Henan in East China (Wang et al., 2014; Quan et  
50 al., 2014; Sun et al., 2014; Yang et al., 2015; Zheng et al., 2016). Studies have shown, however, that models  
51 generally underestimate the explosive growth and peak values of  $PM_{2.5}$  during severe hazes, especially in  
52 Jing–Jin–Ji (Wang et al., 2013; Wang et al., 2014; Li et al., 2016).

53 The causes of  $PM_{2.5}$  explosive growth and its underestimation by atmospheric chemistry models are  
54 complex and uncertain at present, but it possibly involves local emissions, regional transportation, aerosol  
55 physicochemical processes, gas–particle conversion, meteorological conditions, and so on. However, the  
56 actual atmospheric stability and how accurate it is described by atmospheric models is a fundamental  
57 problem that cannot be ignored among others. Local or regional meteorological conditions dictate whether  
58 haze occurs and what the  $PM_{2.5}$  level may be (Zhang et al., 2014; Zheng et al., 2015; Gao et al., 2016) when  
59 source emissions are unchanged for a short period of time. The meteorological conditions of the planetary  
60 boundary layer (PBL) are a key and direct trigger for the emergence of a haze event (Wang et al., 2014; Li  
61 et al., 2016; Zhong et al., 2017). Turbulent diffusion is an important factor to characterize PBL meteorology  
62 when the atmosphere is stable. Also, it is a major pathway of particle and gaseous pollutant exchange from  
63 the surface to upper atmosphere; and when haze occurs, pollutant dispersal via the upper-level winds can  
64 take place when haze is accompanied by calm surface winds and weak vertical motion of air in surface  
65 layers and the PBL. The intensity of turbulent diffusion largely determines the severity of haze pollution.  
66 Thus, a reasonable description of turbulent diffusion by PBL schemes in atmospheric chemistry models is  
67 vital for the prediction of severe pollution (Hong et al., 2006; Wang et al., 2015; Hu et al., 2012, 2013a,  
68 2013b; Li et al., 2016). The latest studies in this field of research show (Wang et al., 2015; Li et al., 2016)  
69 that current PBL schemes may be insufficient for describing the extremely weak turbulent diffusion

70 conditions when extremely severe haze occurs in Jing–Jin–Ji, which more broadly may be one important  
71 reason why PM<sub>2.5</sub> peaks are underestimated by atmospheric chemistry models. More specifically, there may  
72 be two independent reasons why the description of extremely weak turbulent diffusion in atmospheric  
73 models is deficient. One is that aerosol–radiation feedback (AF) is not calculated online in the model run.  
74 AF may restrain turbulence by cooling the surface and PBL while heating the atmosphere above it when  
75 aerosols with certain absorption characteristics are concentrated in the PBL (Wang et al., 2010; Forkel et al.,  
76 2012; Gao et al., 2014, 2015; Wang et al., 2015; Ding et al., 2016; Li et al., 2016; Miao et al., 2016; Petaja  
77 et al., 2016; Gao et al., 2017; Qiu et al., 2017; Zhong et al., 2018). Ignoring AF is likely to lead to an  
78 obvious overestimation of turbulent diffusion when the PM<sub>2.5</sub> concentration exceeds a certain value, which  
79 is worthy of further study. The other possible reason is that the extremely weak turbulence resulting in  
80 extremely severe haze is not fully described by the atmospheric chemistry model (Li et al., 2016).

81 In the present work, a “red-alert” heavy haze event (issued by China’s Ministry of Environmental  
82 Protection when the air pollution index is forecast to exceed 300 over the next three days) that occurred  
83 during 15–23 December 2016 in China’s Jing–Jin–Ji region was selected to study the contributing factors to  
84 PM<sub>2.5</sub> explosive growth and peaks, and the possible deficiency of atmospheric models in describing  
85 extremely weak turbulent diffusion.

## 86 **2 Model, data and methods**

### 87 **2.1 Model**

88 Focusing on dust and haze pollution in China and East Asia, the Chinese Unified Atmospheric  
89 Chemistry Environment (CUACE) (Gong and Zhang, 2008) was online-integrated into the mesoscale  
90 version of the Global/Regional Assimilation and PrEdiction System (GRAPES\_meso), developed by the  
91 Chinese Academy of Meteorological Sciences (Chen et al., 2008; Zhang and Shen, 2008), to build an  
92 online chemical weather forecasting model, GRAPES\_CUACE (Wang et al., 2009, 2010; 2015a; Zhou et  
93 al., 2012). The main components of GRAPES\_CUACE include: a model dynamic core; a modularized  
94 physics package (Xu et al., 2008); an atmospheric chemistry module, CUCAE, with online coupling of  
95 direct and indirect aerosol feedback; and an emissions inventory. The dynamic framework of  
96 GRAPES\_CUACE is semi-implicit, semi-Lagrangian, fully compressible, and non-hydrostatic (Yang et al.,

97 2007, 2008; Chen et al., 2008). A height-based terrain-following coordinate system is used, and there are 33  
98 vertical layers from the surface to 30 km. A longitude–latitude grid is adopted in the spatial discretization of  
99 the model and the horizontal resolution may vary upon request. The physics package can also be tailored by  
100 the user (Xu et al., 2008), and Table 1 lists the specific physics and chemistry schemes used in this study.  
101 The gas-phase chemistry of RAD II (Stockwell et al., 1990), with 63 gaseous species through 21  
102 photochemical reactions and 121 gas-phase reactions, is used in this study. The aerosols include sea salt  
103 (SS), sand/dust (SD), black carbon (BC), organic carbon (OC), sulfates (SFs), nitrates (NI) and ammonium  
104 salts (AM), and aerosol processes involving hygroscopic growth, coagulation, nucleation, condensation,  
105 dry and wet deposition, scavenging, aerosol activation, and so on. The formation of SF aerosols and  
106 secondary organic aerosols from gases, NI and ammonium formed through gaseous oxidation, and  
107 ISORROPIA (Fountoukis et al., 2007) calculating the thermodynamic equilibrium between NI and  
108 ammonium and their gas precursors, are considered in CAUCE, which has been evaluated and introduced  
109 in previous studies (Gong and Zhang et al., 2008; Zhou et al., 2008, 2012).

110 Based on the modeled aerosol concentrations, vertical profiles of temperature change, including direct  
111 aerosol impacts, are calculated by the radiation model and fed back online to the model dynamic core at  
112 each grid point and every time step, which reforms the model temperature field, dynamic process, regional  
113 circulation and meteorological conditions, in turn ultimately impacting the aerosol concentration. The  
114 external mixing of aerosols species (SS, SD, BC, OC, SF, NI, AM) and particle size bins are used in the  
115 calculation of AF, as introduced and evaluated in detail in previous studies (Wang et al., 2009, 2010, 2015a,  
116 2015b). With this two-way GRAPES\_CUACE model, aerosol–radiation–PBL–meteorological interactions,  
117 as well as aerosol–cloud–precipitation interactions and regional pollution and transportation of PM<sub>2.5</sub> etc.,  
118 have been successfully studied (Wang et al., 2010, 2015a, 2015b; Zhou et al., 2012, 2016; Jiang et al., 2015;  
119 Zhang et al., 2018).

120 The turbulent diffusion coefficient (DC) is calculated by the YonSei University PBL scheme (Hong et  
121 al., 2006), which is a revised vertical diffusion package based on the nonlocal boundary layer vertical  
122 diffusion scheme in a medium-range forecast (MRF) model (Hong et al., 1996). The major ingredient of the  
123 revision is the inclusion of an explicit treatment of entrainment processes at the top of the PBL, compared

124 with the MRF PBL scheme. The specific DC calculation method is shown in Hong et al. (1996), and has  
125 been selected as a standard option in MRF models (Caplan et al. 1997; Farfán and Zehnder, 2001; Basu, et  
126 al., 2002; Bright and Mullen, 2002; Mass et al., 2002) as well as the Weather Research and Forecasting  
127 model (Hong et al., 2006) in the National Centers for Environmental Prediction (NCEP) since its  
128 establishment.

129 The horizontal resolution of the model adopted here was  $0.15^\circ \times 0.15^\circ$ , to match the resolution of the  
130 emission source. Considering the impacts of the interregional transport of pollutants, East China ( $100^\circ$ –  
131  $140^\circ\text{E}$ ,  $20^\circ$ – $60^\circ\text{N}$ ) (Figure 1a) was set as the model domain, but our discussion focuses mainly on the most  
132 polluted area, Jing–Jin–Ji (red frame in Figure 1a), for which Figure 1b illustrates the geographical and  
133 topographical features. There are two balloon sounding stations, Xingtai and Beijing (yellow stars in Figure  
134 1b) in our study area. Xingtai, located in southern Hebei province at the eastern foot of the Taihang  
135 Mountains, is influenced by descending airflow from the mountains in winter, and in recent years has  
136 frequently been ranked the most polluted city in China. The topography of Xingtai and the serious haze  
137 pollution it experiences are closely related to its situation on the southern plain of Jing–Jin–Ji. Beijing,  
138 located next to Tianjin and surrounded by Hebei, lies in the transitional zone from the Yan Mountains to its  
139 southern plain, and represents the most polluted areas in the central part of Jing–Jin–Ji.

## 140 **2.2 Emissions inventory**

141 Based on the Multi-resolution Emissions Inventory for China in 2012 (He et al., 2012), the changes in  
142 East China of five kinds of emission sources – industrial, domestic, agricultural, natural, and traffic – were  
143 obtained from national statistical data with respect to industry, energy consumption, road networks, and  
144 motor vehicles, and updated to 2015 and 2016. Five reactive gases ( $\text{SO}_2$ ,  $\text{NO}$ ,  $\text{NO}_2$ ,  $\text{CO}$ ,  $\text{NH}_3$ ), 20 volatile  
145 organic compounds [VOCs ( $\text{ALD}$ ,  $\text{CH}_4$ ,  $\text{CSL}$ ,  $\text{ETH}$ ,  $\text{HC}_3$ ,  $\text{HC}_5$ ,  $\text{HC}_8$ ,  $\text{HCHO}$ ,  $\text{ISOP}$ ,  $\text{KET}$ ,  $\text{NR}$ ,  $\text{OL}_2$ ,  $\text{OLE}$ ,  
146  $\text{OLI}$ ,  $\text{OLT}$ ,  $\text{ORA}_2$ ,  $\text{PAR}$ ,  $\text{TERPB}$ ,  $\text{TOL}$ ,  $\text{XYL}$ ), listed in Table 2], and five aerosol species ( $\text{BC}$ ,  $\text{OC}$ ,  $\text{SF}$ ,  $\text{NI}$   
147 and fugitive dust), were obtained via the above emissions data according to the input requirement of the  
148 CUACE model. The horizontal grid resolution was  $0.15^\circ \times 0.15^\circ$  and there was one emissions dataset for  
149 each month at hourly intervals.

## 150 **2.3 Data**

151 Hourly observational  $PM_{2.5}$  concentration data for more than 1440 surface observational stations (blue  
152 dots in Figure 1) from the China National Environmental Monitoring Centre (<http://www.cnemc.cn>) during  
153 15–23 December 2016 were used to evaluate the model results. The hourly observational meteorological  
154 data, including wind speed and temperature, from 500 surface automatic observation stations of the China  
155 Meteorological Administration (CMA) in the Jing–Jin–Ji region (red triangle in Figure 1b), were used for  
156 model validation. Meteorological balloon sounding data from the CMA at 0000 UTC (early morning) and  
157 1200 UTC (dusk, local time) in Beijing and Xingtai (yellow star in Figure 1b) during the same period were  
158 also used to compare with the modeled results. There is one AERONET station (Holben et al., 1998),  
159 Xianghe, and two CARSNET stations (Che et al., 2009; 2014; 2015), Beijing and Shijiazhuang, in the  
160 Jing–Jin–Ji region (black crosses in Figure 1b). Observed aerosol optical depth (AOD) and single scattering  
161 albedo (SSA) data from these three stations during the same period were also used for model evaluation.  
162 NCEP  $0.25^\circ \times 0.25^\circ$  global analysis gridded data (<https://rda.ucar.edu/datasets/ds083.3>) were used as the  
163 model's initial and six-hourly lateral boundary meteorological input fields. The initial values of chemical  
164 tracers were obtained according to their five-year mean climatic values. The results of the first 120 hours of  
165 the model were discarded to eliminate the effects of the chemical initial fields.

## 166 **2.4 Experimental design**

167 Both dynamic processes of the regional atmosphere and solar radiation have important impacts on  
168 turbulent diffusion and PBL processes. When severe haze occurs, it has been showed from observation  
169 study (Zhong et al., 2018) that surface-level daily direct radiative exposure is reduced by around 89%  
170 compared with clean days, suggesting the possibility of a huge difference in turbulent diffusion between  
171 severe haze and clean days. However, it is difficult to distinguish between the two reasons for extremely  
172 weak turbulent diffusion in the true atmosphere, because of the complicated relationship between  
173 atmospheric dynamics and solar radiation. However, meaningful results might be possible by conducting  
174 sensitivity experiments using an atmospheric chemistry model. Here, three such experiments (EXP1, EXP2,  
175 and EXP3 – see Table 3 for descriptions) were designed to discuss the contributing factors to extremely  
176 weak turbulence and corresponding  $PM_{2.5}$  explosive growth, along with the insufficient description of  
177 extremely weak turbulent diffusion by PBL schemes in atmospheric chemistry models. All other model



178 dynamic processes, physical options, and initial input data of the meteorology and chemical tracers were  
179 same for the three experiments, i.e., except the differences shown in Table 3. In EXP3, a further decrease in  
180 the turbulent diffusion coefficient (DTD) based on EXP2 was only applied to the DC of chemical tracers in  
181 CUACE mode; the DC in other physical packages and the dynamic framework of GRAPES\_MESO was  
182 the same as in EXP1 and EXP2.

### 183 **3 Results and discussion**

184 The studied haze episode began on 15 December 2016.  $PM_{2.5}$  began to gather and climb slowly at this  
185 time, but was below  $150 \text{ ug/m}^3$  in most of Jing–Jin–Ji from 00:00 UTC 15 to 00:00 UTC 17 December – a  
186 period we refer to as the “climbing stage” of  $PM_{2.5}$ . From 00:00 UTC 17 to 00:00 UTC 21 December,  $PM_{2.5}$   
187 increased rapidly, and reaching a peak of  $400\text{--}600 \text{ ug/m}^3$  in most of the study area. We refer to this period  
188 as the “explosive growth stage” of  $PM_{2.5}$ . In this section, we focus mainly on the contributions of AF and  
189 DTD to the  $PM_{2.5}$  during this stage.

#### 190 **3.1 Synoptic background**

191 The circulation in the upper atmosphere and the surface-level synoptic system controlling Jing–Jin–Ji  
192 remained relatively stable during the maintenance of this haze episode. Figure 2 displays the geopotential  
193 height, temperature, and winds in the upper (500 hPa), middle (700 hPa) and lower (850 hPa) atmosphere,  
194 as well as PBL levels (900, 950, 1000 hPa), at 0000 UTC 19 December 2016, to show the meteorological  
195 background. It can be seen that the geopotential height in the upper atmosphere (500 hPa) showed zonal  
196 circulation in East Asia. There was a horizontal trough north of Jing–Jin–Ji (black frame) in the upper and  
197 middle atmosphere (500 and 700 hPa), and the region was controlled by moderate northwesterly or  
198 westerly air flow at the bottom of the trough. The temperature and wind fields at 500 and 700 hPa both  
199 showed that cold air in the upper and middle atmosphere was weak. The 850-hPa geopotential height  
200 showed that the subtropical high in the East Sea was strong; also, Jing–Jin–Ji was in the pressure  
201 equalization field to the northwest periphery of the subtropical high and the wind was very weak at this  
202 level due to the blocking of the subtropical high. The 900-, 950- and 100-hPa geopotential heights all  
203 showed that Jing–Jin–Ji was located in the pressure equalization field between the “northwest land high”  
204 and southeast subtropical high within the whole PBL, and the land high was weaker than the subtropical

205 high. This resulted in a small pressure gradient, weak and thin wind fields, and a stable atmospheric  
206 situation within the PBL, which was conducive to the maintenance of the haze episode.

### 207 **3.2 Observation–model comparison**

208 Meteorological factors not only at the surface but also in the PBL are key in affecting haze processes  
209 and  $PM_{2.5}$  concentrations (Wang et al., 2014a, 2014b). Unfortunately, however, most numerical models  
210 struggle to simulate these aspects, which is also a key point determining the performance of atmospheric  
211 chemistry models (Hu et al., 2013a, 2013b; Li et al., 2016).

212 Using hourly meteorological data from surface automatic observation stations of the CMA, the  
213 surface wind speed and temperature at Beijing and Xingtai, and the average for Jing–Jin–Ji, according to  
214 the results of EXP1, EXP2 and EXP3, were evaluated for the period 15–24 December 2016 (Figure 3). It  
215 can be seen that, in Beijing, the modeled surface wind speed in the three experiments was in good  
216 agreement with observation, in terms of the overall trend as well as the maximum and minimum values.  
217 The observed and modeled wind speed was basically below 2 m/s during 17–21 December (i.e., the  
218 explosive growth stage of  $PM_{2.5}$ ). The modeled wind speed at Xingtai was slightly worse than that at  
219 Beijing, but the overall trend of change was basically consistent with observation, and the wind speed was  
220 also below 2 m/s during the explosive growth stage. The modeled wind speed was to an extent higher than  
221 observed at the beginning and end in Xingtai. The trend of change in the modeled average wind speed for  
222 the Jing–Jin–Ji region showed reasonable agreement with observation and was closest to the observed  
223 situation in the explosive growth stage. In general, the modeled regional wind was higher than observed.  
224 Comparison of the wind speed among the three experiments showed that the wind speeds in EXP2 and  
225 EXP3 were basically same, but to a varying degree both were smaller than in EXP1 at Beijing and Xingtai,  
226 as well as for Jing–Jin–Ji as a whole, during the explosive growth stage, showing that AF decreased the  
227 surface wind speed. The trend of temperature change according to the three experiments was also consistent  
228 with observation, at Beijing, Xingtai, and Jing–Jin–Ji as a whole. However, it was found that the modeled  
229 temperature was obviously higher than observed, especially during the explosive growth stage. The  
230 temperature in EXP2 and EXP3 was basically same, but lower than in EXP1, which was much closer to  
231 observation, indicating that AF reduced the overestimation of surface temperature in Beijing, Xingtai, and

232 Jing–Jin–Ji as a whole. However, the temperature in EXP2 and EXP3 was also higher than observed during  
233 the explosive growth stage, suggesting a role played by other uncertainties in the PBL scheme besides AF,  
234 which is deserving of more detailed study in the future. Also shown in Figure 3 are the PBL-mean winds of  
235 the three experiments for Beijing, Xingtai, and Jing–Jin–Ji as a whole. Unfortunately, no observational data  
236 were available to evaluate them. However, comparison of the PBL’s wind and temperature according to the  
237 three experiments showed that the PBL-mean wind was basically below 4 m/s while the temperature was  
238 high in the explosive stage at Beijing, Xingtai, and in Jing–Jin–Ji as a whole. Similar to the surface-level  
239 results, the PBL-mean wind speed and temperature in EXP2 and EXP3 were basically the same, but the  
240 wind speed in these two experiments was obviously lower than that in EXP1. This indicated that the  
241 reduction in wind speed by AF was more obvious in the PBL than at ground level. Meanwhile, comparison  
242 of the surface-level and PBL temperature of the three experiments showed that the cooling effect of AF was  
243 much stronger at the surface than in the PBL.

244 Aerosol optical properties, including AOD, SSA and asymmetry factor, largely determine the direct  
245 radiative effects of aerosols. The observed AOD (Table 4) and SSA (Table 5) at Shijiazhuang, Beijing and  
246 Xianghe were used to evaluate the modeled results for the period 15–22 December. Because the differences  
247 in the modeled AOD and SSA results of EXP1, EXP2 and EXP3 were small, those of EXP1 only are  
248 referred to here. The values of modeled AOD and SSA and their temporal trends of change during 15–22  
249 December were basically consistent with observation at Beijing, Shijiazhuang and Xianghe, thus  
250 demonstrating good model performance in terms of its description of aerosol optical properties. Both the  
251 observed and modeled SSA at Shijiazhuang, Beijing and Xianghe (Table 5) showed that the SSA was  
252 obviously higher during the explosive growth stage compared with that at the beginning or end of the haze  
253 on 15–16 and 22 December, illustrating that the scattering characteristics of composite aerosols increase  
254 obviously when high AOD and  $PM_{2.5}$  occur on severe haze days in the Jing–Jin–Ji region. The accurate  
255 description of AOD and SSA, especially with respect to the change in SSA from clean to haze days, is the  
256 basis of the following discussion on the effects of aerosols on  $PM_{2.5}$ .

257 Figure 4 displays the averaged observed  $PM_{2.5}$  ( $PM_{2.5\_OBS}$ ) and simulated  $PM_{2.5}$  of EXP1  
258 ( $PM_{2.5\_EXP1}$ ), EXP2 ( $PM_{2.5\_EXP2}$ ) and EXP3 ( $PM_{2.5\_EXP3}$ ) during the explosive growth stage. It can be

259 seen from PM<sub>2.5</sub>\_OBS results that the averaged PM<sub>2.5</sub> values generally exceeded 100 μg/m<sup>3</sup> in east China,  
260 and Jing–Jin–Ji comprised the most polluted areas with PM<sub>2.5</sub> reaching 300–400 μg/m<sup>3</sup> in parts of Beijing,  
261 Tianjin, central-south Hebei, western Shandong, and northern Henan. The most polluted area with PM<sub>2.5</sub>  
262 values of 500–700 μg/m<sup>3</sup> appeared in southern Hebei and northern Henan provinces and the maximum  
263 value of PM<sub>2.5</sub> even exceeded 700 μg/m<sup>3</sup> in part area in southern Hebei. Comparison of PM<sub>2.5</sub>\_EXP1 and  
264 PM<sub>2.5</sub>\_OBS shows that PM<sub>2.5</sub>\_EXP1 was obviously lower than PM<sub>2.5</sub>\_OBS on the whole. Notably, EXP1  
265 failed to simulate the PM<sub>2.5</sub> > 300 μg/m<sup>3</sup>. PM<sub>2.5</sub>\_OBS was approximately 200–300 μg/m<sup>3</sup> over most of  
266 Shandong, while PM<sub>2.5</sub>\_bk was only 100–200 μg/m<sup>3</sup> in this region. Compared with PM<sub>2.5</sub>\_EXP1, the  
267 PM<sub>2.5</sub>\_EXP2 values were significantly improved by AF, and were much closer to PM<sub>2.5</sub>\_OBS. The high  
268 PM<sub>2.5</sub>\_OBS centers of 300–400, 400–500 and 500–600 μg/m<sup>3</sup> were almost simulated by EXP2, indicating  
269 the important effects of AF in simulating such high values of PM<sub>2.5</sub>. However, the simulated areas of these  
270 centers were smaller than those of PM<sub>2.5</sub>\_OBS. EXP2 also failed to simulate the maximum PM<sub>2.5</sub> values  
271 over 600 μg/m<sup>3</sup> observed in southern Hebei. PM<sub>2.5</sub>\_EXP3 just about made up for this shortcoming;  
272 compared with PM<sub>2.5</sub>\_EXP1 and PM<sub>2.5</sub>\_EXP2, PM<sub>2.5</sub>\_EXP3 was undoubtedly the closest to PM<sub>2.5</sub>\_OBS  
273 both in terms of PM<sub>2.5</sub> extremes and the area of influence. These findings illustrate that both AF and DTD  
274 in atmospheric chemistry models are required for the effective prediction of PM<sub>2.5</sub> explosive growth during  
275 severe haze in China’s Jing–Jin–Ji region.

### 276 **3.3 Change in downward solar radiation flux by aerosols and DTD**

277 PM in the atmosphere will inevitably lead to changes in surface and atmospheric solar radiation flux.  
278 When severe haze occurs, most PM is concentrated in the atmosphere near the surface and within the PBL;  
279 solar radiative flux reaching the ground is reduced greatly, which is a direct trigger for the subsequent  
280 changes in thermodynamics, dynamics, and then atmospheric stratification. Any factor leading to a change  
281 in the atmospheric PM loading might result in a change in the surface downward solar radiation flux  
282 (SDSRF). We calculated the percentage changes in SDSRF (W/m<sup>2</sup>) between EXP2 and EXP1  
283  $[(\text{SDSRF}_{\text{EXP2}} - \text{SDSRF}_{\text{EXP1}}) / \text{SDSRF}_{\text{EXP1}}]$ , and EXP3 and EXP1  $[(\text{SDSRF}_{\text{EXP3}} - \text{SDSRF}_{\text{EXP1}}) /$   
284  $\text{SDSRF}_{\text{EXP1}}]$ , to study the impacts on SDSRF of aerosols and DTD. Figure 5 shows the mean percentage  
285 change in SDSRF (W/m<sup>2</sup>) owing to aerosols (a) and aerosols plus DTD, during the explosive growth stage.

286 It can be seen that SDSRF was reduced by more than 50% by aerosols over most of the study region (60%–  
287 65% in Jing, Jin, most of Ji, and northern Shandong, and even 65%–70% in Jing, Jin, and part of Ji),  
288 indicating the important influence of aerosols on SDSRF. Comparison of Figures 5b and 5a shows that this  
289 reduction in SDSRF owing to aerosols (Figure 5a) in EXP2 was further strengthened by the DTD of  
290 chemical tracers in EXP3 (Figure 5b) in certain regions, because DTD led to the accumulation of more  
291  $PM_{2.5}$  near the surface (Figure 3), less transport and, subsequently, an increase in total  $PM_{2.5}$  loading. It can  
292 also be seen that the difference between Figures 5a and 5b is negligible. This is because the major impact of  
293 DTD was to reform the vertical distribution of the atmospheric loading of  $PM_{2.5}$ , and its impact on the  
294 total-column  $PM_{2.5}$  was minor. On the other hand, the reduction in SDSRF owing to aerosol radiation was  
295 already considerable, and so the change in SDSRF owing to the increased total-column  $PM_{2.5}$  by DTD  
296 would be secondary. This value of SDSRF reduction owing to aerosols and DTD is basically consistent  
297 with the 56%–89% difference of observational radiative exposure between clear and haze days during the  
298 same period (Zhong et al., 2018).

#### 299 **3.4 Influence of aerosols on the reforming of the local atmospheric temperature profile**

300 Offline and online studies indicate a reforming of the atmospheric temperature profile owing to the  
301 direct effect of aerosol radiation (Wang et al., 2010, 2015b; Forkel et al., 2012; Gao et al., 2014, 2015;  
302 Wang et al., 2014; Gao et al., 2017; Ding et al., 2016). In our previous work (Wang et al., 2015a, 2015b),  
303 composite aerosol mixing of BC, OC, SF, NI, dust, ammonium, and sea salt aerosols was online coupled  
304 into the GRAPES\_CAUCE model. On this basis, in the present study, the changes in the mean temperature  
305 profile of Jing–Jin–Ji during daytime owing to aerosol radiation were calculated for 15–20 December 2016.  
306 It can be seen from Figure 6 that aerosols cooled the atmosphere below 750–800 hPa, but warmed it above  
307 this height. Considering the PBL height may be as low as several hundreds to one thousand meters when  
308 severe haze occurs in Jing–Jin–Ji (Wang et al., 2015a; Zhong et al., 2017), it may be concluded that the  
309 whole PBL and its near upper atmosphere were cooled by aerosols to a varying extent during the different  
310 stages of this haze process. The warming effects of aerosols above 750–850 hPa were very weak, and the  
311 temperature differences among different days were also small. However, the cooling effects of aerosols  
312 varied the most between different days from the surface to 975 hPa. For instance, surface daytime cooling

313 was about 2.2 K on 19 December, 1.5 K on 18 and 20 December, 1 K on 17 December, and 0.5–0.6 K on  
314 15–16 December. This cooling effect of aerosols decreased rapidly with height. The difference in the  
315 cooling rate between the surface and 850 hPa was 1.8 K on 19 December, 1.3 K on 18 and 20 December, 1  
316 K on 17 December, and 0.3–0.4 K on 15 and 16 December. The difference in the cooling rate owing to  
317 aerosols between the surface and the upper PBL was much bigger during the explosive growth stage than  
318 the climbing stage. This may have resulted in further intensification of the temperature inversion layer that  
319 already existed during the haze event, which will be discussed in the following section.

320 The meteorological data from the vertical soundings taken at Beijing and Xingtai were used to verify  
321 this change in the temperature profile owing to aerosols. Figure 7 shows the vertical temperature profiles of  
322 the sounding observations and the modeled temperature profiles of EXP1 and EXP2 during the climbing  
323 stage (Figure 7a) and explosive growth stage (Figure 7b) at the two stations. The temperature profiles  
324 (Figure 7a) show that the model results of EXP1 and EXP2 both simulated in part the observed temperature  
325 inversion at Beijing and Xingtai on 15–16 December. The negligible difference between the temperature  
326 profiles of EXP1 and EXP2 indicates that aerosol radiation had very little impact on the temperature  
327 profiles and local inversion during the climbing stage. Nevertheless, Figure 7b shows that the observed  
328 temperature inversions were obviously stronger and thicker on 18–19 December (explosive growth stage)  
329 than those on 15–16 (climbing stage), both in Xingtai and Beijing. The temperature profiles of EXP2 were  
330 much closer to the observational results than those of EXP1; and especially, the temperature inversions  
331 were much stronger and also closer to observation than those of EXP1. This result proves that the  
332 correction of local inversions by aerosols during the PM<sub>2.5</sub> explosive growth stage was effective.

333 However, it can also be seen that the inversions of EXP2, which included online AF, were still  
334 weaker than observed at the two stations. This suggests there must be other reasons, besides the online  
335 calculation of AF, for the underestimation of the observed extremely strong inversion by the model, which  
336 is worthy of further study.

### 337 **3.5 Contributions of AF and DTD to PM<sub>2.5</sub> explosive growth**

338 Turbulent diffusion is the main process of gas and particle exchange from surface to upper atmosphere,  
339 and removal by high-altitude transport, and one of the key tasks of atmospheric chemistry models is to

340 capture this process. Firstly, the inversion and weak turbulent diffusion, which generates from atmospheric  
341 dynamic processes, leads to atmospheric stabilization and determines the occurrence of haze and its  
342 strength (Zheng et al., 2016). Once the haze occurs, aerosol radiation may in turn reinforce the inversion  
343 when aerosols exceed a certain critical value, leading to more  $PM_{2.5}$  gathering near the ground. The relative  
344 importance of these two aspects on  $PM_{2.5}$  explosive growth may vary with  $PM_{2.5}$  concentrations and  
345 meteorological conditions, but they are irreplaceable for a reasonable prediction and simulation of  $PM_{2.5}$   
346 explosive growth and peaks in atmospheric models.

347 Figure 8 displays the hourly change in observed  $PM_{2.5}$  ( $PM_{2.5\_OBS}$ ) and the modeled  $PM_{2.5}$  of EXP1,  
348 EXP2 and EXP3, together with the modeled turbulent DC of the three experiments, in Beijing (Figure 8a)  
349 and Xingtai (Figure 8b), for the period 15–23 December. Comparison of the  $PM_{2.5}$  modeled by EXP1,  
350 EXP2 and EXP3 with observation in Beijing (Figure 8a) shows that the  $PM_{2.5}$  modeled by EXP3 was the  
351 closest to observation during the whole haze episode, which agreed with the results of the regional  
352 distribution of the explosive growth stage illustrated in Figure 4. EXP1 underestimated the  $PM_{2.5}$  obviously  
353 during 17–22 December, and this underestimation was even more obvious with increasing  $PM_{2.5}$ . This  
354 difference between the modeled and observed  $PM_{2.5}$  was largest during the explosive growth stage. AF  
355 reduced this difference to a considerable extent, and the  $PM_{2.5}$  of EXP2 was much closer to observation  
356 than that of EXP1 during the explosive growth stage. However, there were certain differences between the  
357 observed and  $PM_{2.5}$  and that modeled by EXP2, illustrating that AF cannot completely fill the sizeable gap  
358 between observed and modeled  $PM_{2.5}$ . The  $PM_{2.5}$  of EXP3 reduced this gap further, showing the best  
359 agreement with observation, especially during the  $PM_{2.5}$  explosive growth stage.

360 It can also be seen from Figure 8a that the DC of EXP1 was about 30–40  $m^2/s$  during the explosive  
361 growth stage, which was about 50% of the 60–70  $m^2/s$  on clear days (15 or 22 December). Obviously, this  
362 50% DC difference between clear and severe haze days may be insufficient to separate the difference in  
363 turbulent diffusion intensity between the extremely stable atmosphere on haze days and the unstable  
364 atmosphere on clear days, which is an important reason for the underestimated  $PM_{2.5}$  explosive growth in  
365 EXP1. Compared with EXP1, the AF in EXP2 led to a notable enhancement of the temperature inversion  
366 (Figure 7b), a significant decrease in the turbulent diffusion of  $PM_{2.5}$  during the explosive growth stage, and

367 a low maximum DC at noon (as low as  $14 \text{ m}^2/\text{s}$  on 20 December – a reduction of 50% compared with  
368 EXP1). The maximum DC at noon on haze days in EXP2 was only about 20% of that on clear days. The  
369 maximum DC at noon in EXP3 was lower than  $5 \text{ m}^2/\text{s}$  on 20 December and, at the same time, the  $\text{PM}_{2.5}$   
370 modeled by EXP3 was further increased and was also much closer to the observed  $\text{PM}_{2.5}$  than the  $\text{PM}_{2.5}$  of  
371 EXP2.

372 Through comparison of the temporal change of DC and  $\text{PM}_{2.5}$  in EXP1, EXP2 and EXP3 in Beijing, it  
373 is clear that an overestimation of turbulent DC owing to the absence of online-calculated AF, as well as a  
374 deficient description of extremely stable stratification in the PBL scheme of the atmospheric model, can  
375 lead to a distinct underestimation of  $\text{PM}_{2.5}$  explosive growth and peaks when severe haze occurs in China's  
376 Jing–Jin–Ji region.

377 The trends of change in DC and  $\text{PM}_{2.5}$  at Xingtai in the three experiments (Figure 8b) are similar to  
378 those at Beijing. The  $\text{PM}_{2.5}$  of EXP3 was also closest to observation, followed by EXP2, and then EXP1  
379 was the worst, during the whole haze episode. However, during the explosive growth stage, the relative  
380 contributions of AF and DTD to the  $\text{PM}_{2.5}$  peak values showed some differences to those at Beijing. The  
381 contributions of DTD to  $\text{PM}_{2.5}$  peaks were more important than those of AF at Xingtai. Located in the  
382 eastern foothills of the Taihang Mountains, Xingtai is usually affected by downhill airflow. Temperature  
383 inversions in this area form and strengthen easily, leading to stronger inversion, weaker turbulent diffusion,  
384 and more stable atmospheric stratification. However, this kind of inversion and weak turbulent diffusion,  
385 derived from the local terrain, is harder for PBL schemes in atmospheric chemistry models to describe, and  
386 likely underestimated.

387 Figure 9 is a diagrammatic sketch of the contributions of AF and DTD to the  $\text{PM}_{2.5}$  of the explosive  
388 growth stage according to the results at Beijing and Xingtai. It can be seen that the DC of EXP1 was 30–35  
389  $\text{m}^2/\text{s}$ , while that of EXP2 was 15–17  $\text{m}^2/\text{s}$ , meaning AF reduced the DC by about 43%–57%, which led to  
390 the rise in simulated  $\text{PM}_{2.5}$  from  $144 \text{ ug}/\text{m}^3$  in EXP1 to  $205 \text{ ug}/\text{m}^3$  in EXP2 at Beijing, and from  $280 \text{ ug}/\text{m}^3$   
391 in EXP1 to  $360 \text{ ug}/\text{m}^3$  in EXP2 at Xingtai. This means that AF reduced the underestimation of  $\text{PM}_{2.5}$  at  
392 Beijing and Xingtai by 20% and 25%, respectively. The DC of EXP3 was as low as 4–6  $\text{m}^2/\text{s}$  during the  
393 explosive growth stage, demonstrating the joint effects of AF and DTD reduced the DC to less than 4–6



394  $\text{m}^2/\text{s}$ , near-zero, which we refer to as “turbulent intermittence”. The direct result of this “turbulent  
395 intermittence” was a further increase in the simulated surface  $\text{PM}_{2.5}$ , based on EXP2. DTD reduced the  
396 underestimation of simulated  $\text{PM}_{2.5}$  by 14% to 20%, and the  $\text{PM}_{2.5}$  errors in EXP3 were reduced to as low  
397 as -11% to 2%.

#### 398 4. Conclusions

399 Using an atmospheric chemistry model, GRAPES\_CUACE, three experiments (EXP1, EXP2 and  
400 EXP3) were designed to study the reason for the explosive growth of  $\text{PM}_{2.5}$  mass during a “red-alert” heavy  
401 haze event that occurred during 15–23 December 2016 in China’s Jing–Jin–Ji region. The contributions of  
402 AF and DTD to the  $\text{PM}_{2.5}$ , representing compensation for the deficient description of extremely weak  
403 turbulent diffusion in the PBL scheme of the atmospheric model, were studied by analyzing the changes in  
404  $\text{PM}_{2.5}$ , SDSRF, wind speed and temperature, DC, and the relationships among them, in the three  
405 experiments.

406 Results show that the DC in EXP1 was about 60–70  $\text{m}^2/\text{s}$  on clear days and 30–35  $\text{m}^2/\text{s}$  on haze days.  
407 The 50% difference between the two was considered insufficient to separate the unstable atmosphere on  
408 clear days and the extreme stable atmosphere on severe haze days, compared with the differences in direct  
409 downward solar radiation between clear and haze days, which was also proven indirectly by the weaker  
410 inversion of EXP1 than that from sounding observations. This led to a 40%–51% underestimation of the  
411  $\text{PM}_{2.5}$  peaks in EXP1 during the  $\text{PM}_{2.5}$  explosive growth stage. Online calculation of AF reduced the surface  
412 and PBL wind speed and cooled the surface and PBL atmosphere. The surface daytime cooling due to  
413 aerosol radiation was 1.5–2.2 K during the explosive growth stage and 0.5–0.6 K during the climbing stage.  
414 The cooling effect of aerosols decreased rapidly with height, and this was a major reason for the  
415 strengthening of the temperature inversion during the explosive growth stage. The reduced DC owing to AF  
416 reached 43%–57% during the  $\text{PM}_{2.5}$  explosive growth stage. The local inversion simulated in EXP2 was  
417 strengthened and closer to the actual sounding observation than that of EXP1. This resulted in a 20%–25%  
418 reduction in the underestimation of  $\text{PM}_{2.5}$ , with  $\text{PM}_{2.5}$  errors in EXP2 being as low as -16 to -11% during  
419 the explosive growth stage. The impact on  $\text{PM}_{2.5}$  owing to AF in the model run was distinct during the  
420 explosive growth stage, but minor during the climbing stage, indicating a critical value of  $150 \text{ ug}/\text{m}^3$  of

421  $PM_{2.5}$  leading to an effective AF in online atmospheric chemistry models. However, the local inversion  
422 simulated by EXP2 was still weaker than observed, and the  $PM_{2.5}$  of EXP2 was still smaller than observed,  
423 illustrating AF could not solve all the  $PM_{2.5}$  underestimation problems. In EXP3, the DTD of particles and  
424 gas based on EXP2 resulted in a 14%–20% lessening of the  $PM_{2.5}$  underestimation based on EXP2, and the  
425  $PM_{2.5}$  errors of EXP3 were reduced to –11% to 2%.

426 The present study illustrates that the PBL schemes in current atmospheric chemistry models are  
427 probably insufficient for describing the extremely stable atmosphere resulting in explosive growth of  $PM_{2.5}$   
428 and severe haze in China’s Jing–Jin–Ji region. This may involve two important reasons: the absence of an  
429 online calculation of AF, and/or a deficient description of extremely weak turbulent diffusion by the PBL  
430 scheme in the atmospheric chemistry model. Our study suggests that an online calculation of AF and an  
431 improvement in the representation of turbulent diffusion in PBL schemes, with a focus on extremely stable  
432 atmospheric stratification, in atmospheric chemistry models, are indispensable for a reasonable description  
433 of local “turbulent intermittence” and an accurate prediction of the explosive growth and peaks of  $PM_{2.5}$  of  
434 severe haze in China’s Jing–Jin–Ji region.

435

436

437 **Author Contributions:**

438 Hong Wang and Xiaoye Zhang designed the idea and experiments; Hong Wang and Yue Peng carried them  
439 out; Hongli Liu prepared the emissions data and introduction; Meng Zhang performed some of the model  
440 runs; Huizheng Che and Yu Zheng processed the AOD and SSA observational data; Yanli Cheng completed  
441 Table 3 and the related introduction.

442 **Acknowledgements**

443 This study was supported by the National Key Project (2016YFC0203306), the National Natural Science  
444 Foundation of China (41590874), and the National (Key) Basic Research and Development (973) Program  
445 of China (2014CB441201).

446 **References**

- 447 Basu, S., Iyengar, G. R., and Mitra, A. K.: Impact of a nonlocal closure scheme in a simulation of a  
448 monsoon system over India. *Mon. Wea. Rev.*, 130, 161–170, 2002.
- 449 Bright, D. R., and Mullen, S. L.: The sensitivity of the numerical simulation of the southwest monsoon  
450 boundary layer to the choice of PBL turbulence parameterization in MM5, *Wea. Forecasting*, 17, 99–  
451 114, 2002.
- 452 Caplan, P., Derber, J., Gemmill, W., Hong, S.-Y., Pan, H.-L., and Parrish, D.: Changes to the 1995 NCEP  
453 operational medium-range forecast model analysis-forecast system, *Wea. Forecasting*, 12, 581–594,  
454 1997.
- 455 Che, H., Zhang, X., Chen, H., Damiri, B., Goloub, P., Li, Z., Zhang, X., Wei, Y., Zhou, H., Dong, F., Li, D.,  
456 and Zhou, T.: Instrument calibration and aerosol optical depth validation of the China Aerosol Remote  
457 Sensing Network, *J. Geophys. Res. Atmos.*, 114, D03206, doi:10.1029/2008JD011030, 2009.
- 458 Che, H., Xia, X., Zhu, J., Li, Z., Dubovik, O., Holben, B., Goloub, P., Chen, H., Estelles, V., Cuevas-Agulló,  
459 E., Blarel, L., Wang, H., Zhao, H., Zhang, X., Wang, Y., Sun, J., Tao, R., Zhang, X., and Shi, G.:  
460 Column aerosol optical properties and aerosol radiative forcing during a serious haze-fog month over  
461 North China Plain in 2013 based on ground-based sunphotometer measurements, *Atmos. Chem. Phys.*,  
462 14, 2125–2138, doi:10.5194/acp-14-21252014, 2014.
- 463 Che, H., Zhang, X.-Y., Xia, X., Goloub, P., Holben, B., Zhao, H., Wang, Y., Zhang, X. C., Wang, H., Blarel,

464 L., Damiri, B., Zhang, R., Deng, X., Ma, Y., Wang, T., Geng, F., Qi, B., Zhu, J., Yu, J., Chen, Q., and  
465 Shi, G.: Ground-based aerosol climatology of China: aerosol optical depths from the China Aerosol  
466 Remote Sensing Network (CARSNET) 2002–2013, *Atmos. Chem. Phys.*, 15, 7619–7652,  
467 <https://doi.org/10.5194/acp15-7619-2015>, 2015.

468 Chen, D., Xue, J., Yang, X., Zhang, H., Shen, X., Hu, J., Wang, Y., Ji, L., and Chen, J.: New generation of  
469 multi-scale NWP system (GRAPES): general scientific design, *Chinese Sci. Bull.*, 53, 3433–3445,  
470 doi:10.1007/s11434-008-0494-z, 2008.

471 Chou, M. D., Suarez, M. J., Ho, C. H., Yan, M. M. H., and Lee, K. T.: Parameterizations for Cloud  
472 Overlapping and Shortwave Single-Scattering Properties for Use in General Circulation and Cloud  
473 Ensemble Models, *J. Clim.*, 11, 202–214, 1998.

474 Chou, M. D., Suarez, M. J., Liang, X. Z., and Michael M.-H. Y.: A Thermal Infrared Radiation  
475 Parameterization for Atmospheric Studies, Technical Report Series on Global Modeling and Data  
476 Assimilation, NASA/TM-2001-104606, 19, America, Goddard Space Flight Center, Greenbelt,  
477 Maryland, 55, 2001.

478 Ding, A. J., Fu, C. B., Yang, X. Q., Sun, J. N., Petäjä, T., Kerminen, V. M., Wang, T., Xie, Y., Herrmann, E.,  
479 Zheng, L. F., Nie, W., Liu, Q., Wei, X. L., and Kulmala, M.: Intense atmospheric pollution modifies  
480 weather: a case of mixed biomass burning with fossil fuel combustion pollution in eastern China,  
481 *Atmos. Chem. Phys.*, 13, 10545-10554, 2013.

482 Ding, A. J., Huang, X., Nie, W., Sun, J. N., Kerminen, V. M., Petäjä, T., Su, H., Cheng, Y. F., Yang, X. Q.,  
483 Wang, M. H., Chi, X. G., Wang, J. P., Virkkula, A., Guo, W. D., Yuan, J., Wang, S. Y., Zhang, R. J., Wu,  
484 Y. F., Song, Y., Zhu, T., Zilitinkevich, S., Kulmala, M., and Fu, C. B.: Enhanced haze pollution by  
485 black carbon in megacities in China, *Geophys. Res. Lett.*, 43, 2873-2879, 2016.

486 Farfán, L. M., and Zehnder, J. A.: An analysis of the landfall of Hurricane Nora (1997), *Mon. Wea. Rev.*,  
487 129, 2073–2088, 2001.

488 Forkel, R., Werhahn, J., Hansen, A. B., McKeen, S., Peckham, S., Grell, G., and Suppan, P.: Effect of  
489 aerosol-radiation feedback on regional air quality – A case study with WRF/Chem, *Atmos. Environ.*,  
490 53, 202-211, 2012.

491 Fountoukis, C., and Nenes A., ISORROPIA II: a computationally efficient thermodynamic equilibrium  
492 model for  $K^+$ – $Ca^{2+}$ – $Mg^{2+}$ – $NH_4^+$  – $Na^+$ – $SO_4^{2-}$  – $NO_3^-$  – $Cl^-$ – $H_2O$  aerosols, *Atmos. Chem. Phys.*,  
493 2007, 7, 4639–4659.

494 Gal-Chen, T., and Somerville, R. C. J.: On the use of a coordinate transformation for the solution of the  
495 Navier-Stokes equations, *J. Comput. Phys.*, 17, 209–228, 1975.

496 Gao, Y., Zhao, C., Liu, X., Zhang, M., and Leung, L. R.: WRF-Chem simulations of aerosols and  
497 anthropogenic aerosol radiative forcing in East Asia, *Atmos. Environ.*, 92, 250-266, 2014.

498 Gao, Y., Zhang, M., Liu, Z., Wang, L., Wang, P., Xia, X., Tao, M., and Zhu, L.: Modeling the feedback  
499 between aerosol and meteorological variables in the atmospheric boundary layer during a severe fog–  
500 haze event over the North China Plain, *Atmos. Chem. Phys.*, 15, 4279-4295, 2015.

501 Gao, M., Carmichael, G. R., Saide, P. E., Lu, Z., Yu, M., Streets, D. G., and Wang, Z.: Response of winter  
502 fine particulate matter concentrations to emission and meteorology changes in North China, *Atmos.*  
503 *Chem. Phys.*, 16, 11837-11851, 2016.

504 Gao, M., Saide, P. E., Xin, J., Wang, Y., Liu, Z., Wang, Y., Wang, Z., Pagowski, M., Guttikunda, S.K., and  
505 Carmichael, G. R.: Estimates of Health Impacts and Radiative Forcing in Winter Haze in Eastern  
506 China through Constraints of Surface PM<sub>2.5</sub> Predictions, *Environ. Sci. Technol.*, 51, 2178-2185, 2017.

507 Gong, S., and Zhang, X.: CUACE/Dust-an integrated system for operational dust forecasting in Asia,  
508 *Computers & Applied Chemistry*, 25, 1061-1067, 2008.

509 Gong, S. L., Lavoué, D., Zhao, T. L., Huang, P., and Kaminski, J. W.: GEM-AQ/EC, an on-line global  
510 multi-scale chemical weather modelling system: model development and evaluation of global aerosol  
511 climatology, *Atmos. Chem. Phys.*, 12, 8237–8256, doi:10.5194/acp-12-8237-2012, 2012.

512 Grell, G. A., Dudhia, J., and Stauffer, D.: A description of the fifth-generation PENN State/NCAR  
513 Mesoscale Model (MM5). NCAR Tech. Note NCAR/TN-398 STR, 138, 1994.

514 He, K.: Multi-resolution Emission Inventory for China (MEIC): model framework and 1990-2010  
515 anthropogenic emissions, AGU Fall Meeting, AGU Fall Meeting Abstracts, 2012.

516 Holben B. N., Eck, T .F., Slutsker, I., et al. AERONET—A Federated Instrument Network and Data  
517 Archive for Aerosol Characterization, 1998.

518 Hong, S. Y. and Pan, H. L.: Nonlocal boundary layer vertical diffusion in a Medium-Range Forecast model,  
519 Mon. Weather Rev., 124, 2322–2339, 1996.

520 Hong, S. Y., Noh, Y., and Dudhia, J.: A New Vertical Diffusion Package with an Explicit Treatment of  
521 Entrainment Processes, Mon. Weather Rev., 134, 2318-2341, 2006.

522 Hu, X. M., Doughty, D. C., Sanchez, K. J., Joseph, E., and Fuentes, J. D.: Ozone variability in the  
523 atmospheric boundary layer in Maryland and its implications for vertical transport model, Atmos.  
524 Environ., 46, 354-364, 2012.

525 Hu, X. M., Klein, P. M., and Xue, M.: Evaluation of the updated YSU planetary boundary layer scheme  
526 within WRF for wind resource and air quality assessments, J. Geophys. Res. Atmos., 118,  
527 10490-10505, 2013a.

528 Hu, X. M., Klein, P. M., Xue, M., Zhang, F., Doughty, D. C., Forkel, R., Joseph, E., and Fuentes, J. D.:  
529 Impact of the vertical mixing induced by low-level jets on boundary layer ozone concentration, Atmos.  
530 Environ., 70, 123-130, 2013b.

531 Hua, Y., Wang, S., Wang, J., Jiang, J., Zhang, T., Song, Y., Kang, L., Zhou, W., Cai, R., Wu, D., Fan, S.,  
532 Wang, T., Tang, X., Wei, Q., Sun, F., and Xiao, Z.: Investigating the impact of regional transport on  
533 PM<sub>2.5</sub> formation using vertical observation during APEC 2014 Summit in Beijing, Atmos. Chem.  
534 Phys., 16, 15451–15460, 2016.

535 Huang, R. J., Zhang, Y., Bozzetti, C., Ho, K. F., Cao, J. J., Han, Y., Daellenbach, K. R., Slowik, J. G., Platt,  
536 S. M., Canonaco, F., Zotter, P., Wolf, R., Pieber, S. M., Bruns, E. A., Crippa, M., Ciarelli, G.,  
537 Piazzalunga, A., Schwikowski, M., Abbaszade, G., Schnelle-Kreis, J., Zimmermann, R., An, Z., Szidat,  
538 S., Baltensperger, U., El Haddad, I., and Prevot, A. S.: High secondary aerosol contribution to  
539 particulate pollution during haze events in China, Nature, 514, 218-222, 2014.

540 Jiang, C., Wang, H., Zhao, T., Li, T., and Che, H.: Modeling study of PM<sub>2.5</sub> pollutant transport across cities  
541 in China's Jing–Jin–Ji region during a severe haze episode in December 2013, Atmos. Chem. Phys., 15,  
542 5803-5814, 2015.

543 Kain, J. S. and Fritsch, J. M.: Convection parameterization for mesoscale models: the Kain-Fritsch scheme,  
544 Meteor. Mon., 24, 165–170, 1993.

545 Kusaka, H., Kondo, H., Kikegawa, Y., and Kimura, F.: A simple single-layer urban canopy model for  
546 atmospheric models: Comparison with multi-layer and slab models. *Bound.-Layer Meteor.*, 101, 329–  
547 358, 2001.

548 Li, K., Liao, H., Zhu, J., and Moch, J. M.: Implications of RCP emissions on future PM<sub>2.5</sub> air quality and  
549 direct radiative forcing over China, *J. Geophys. Res. Atmos.*, 121, 12985-13008, 2016.

550 Li, T., Wang, H., Zhao, T., Xue, M., Wang, Y., Che, H., and Jiang, C.: The Impacts of Different PBL  
551 Schemes on the Simulation of PM<sub>2.5</sub> during Severe Haze Episodes in the Jing-Jin-Ji Region and Its  
552 Surroundings in China, *Adv. Meteorol.*, 1-15, 2016.

553 Lim, K. S. S., and Hong, S. Y.: Development of an effective double-moment cloud microphysics scheme  
554 with prognostic cloud condensation nuclei (CCN) for weather and climate models, *Mon. Wea. Rev.*,  
555 138, 1587-1612, 2010.

556 Mass, C. F., D. Ovens, K. Westrick, and B. A. Colle: Does increasing horizontal resolution produce more  
557 skillful forecasts? *Bull. Amer. Meteor. Soc.*, 83, 407–430, 2002.

558 Miao, Y., Liu, S., Zheng, Y., and Wang, S.: Modeling the feedback between aerosol and boundary layer  
559 processes: a case study in Beijing, China, *Environ. Sci. Pollut R.*, 23, 3342-3357, 2016.

560 Petäjä, T., Järvi, L., Kerminen, V. M., Ding, A. J., Sun, J. N., Nie, W., Kujansuu, J., Virkkula, A., Yang, X.  
561 Q., Fu, C. B., Zilitinkevich, S., and Kulmala, M.: Enhanced air pollution via aerosol-boundary layer  
562 feedback in China, *Sci. Rep.*, 6, 18998, 2016.

563 Pleim, J.: A combined local and non-local closure model for the atmospheric boundary layer. Part II:  
564 Application and evaluation in a mesoscale meteorological model, *J. Applied Meteor. Climatology*, 46,  
565 1396–1409, 2007.

566 Qiu, Y., Liao, H., Zhang, R., and Hu, J.: Simulated impacts of direct radiative effects of scattering and  
567 absorbing aerosols on surface layer aerosol concentrations in China during a heavily polluted event in  
568 February 2014, *J. Geophys. Res. Atmos.*, 122, 5955-5975, 2017.

569 Quan, J., Tie, X., Zhang, Q., Liu, Q., Li, X., Gao, Y., and Zhao, D.: Characteristics of heavy aerosol  
570 pollution during the 2012–2013 winter in Beijing, China, *Atmos. Environ.*, 88, 83-89, 2014.

571 Stockwell, W. R., Middleton, P., Chang, J. S., and Tang, X.: The Second Generation Regional Acid

572 Deposition Model Chemical Mechanism for Regional Air Quality Modeling, *J. Geophys. Res.*, 95,  
573 16343-16376, 1990.

574 Sun, Y., Jiang, Q., Wang, Z., Fu, P., Li, J., Yang, T., and Yin, Y.: Investigation of the sources and evolution  
575 processes of severe haze pollution in Beijing in January 2013, *J. Geophys. Res. Atmos.*, 119,  
576 4380-4398, 2014.

577 Wang, H., Gong, S., Zhang, H., Chen, Y., Shen, X., Chen, D., Xue, J., Shen, Y., Wu, X., and Jin, Z.: A  
578 new-generation sand and dust storm forecasting system GRAPES\_CUACE/Dust: Model development,  
579 verification and numerical simulation, *Chinese Sci. Bull.*, 55, 635-649, 2009.

580 Wang, H., Zhang, X., Gong, S., Chen, Y., Shi, G., and Li, W.: Radiative feedback of dust aerosols on the  
581 East Asian dust storms, *J. Geophys. Res.*, 115 , D23214, 2010.

582 Wang, H., Tan, S. C., Wang, Y., Jiang, C., Shi, G. Y., Zhang, M. X., and Che, H. Z.: A multi sources  
583 observation study of the severe prolonged regional haze episode over eastern China in January 2013,  
584 *Atmos. Environ.*, 89, 807-815, 2014a.

585 Wang, H., Xu, J., Zhang, M., Yang, Y., Shen, X., Wang, Y., Chen, D., and Guo, J.: A study of the  
586 meteorological causes of a prolonged and severe haze episode in January 2013 over central-eastern  
587 China, *Atmos. Environ.*, 98, 146-157, 2014b.

588 Wang, H., Xue, M., Zhang, X. Y., Liu, H. L., Zhou, C. H., Tan, S. C., Che, H. Z., Chen, B., and Li, T.:  
589 Mesoscale modeling study of the interactions between aerosols and PBL meteorology during a haze  
590 episode in Jing-Jin-Ji (China) and its nearby surrounding region – Part 1: Aerosol distributions and  
591 meteorological features, *Atmos. Chem. Phys.*, 15, 3257-3275, 2015a.

592 Wang, H., Shi, G. Y., Zhang, X. Y., Gong, S. L., Tan, S. C., Chen, B., Che, H. Z., and Li, T.: Mesoscale  
593 modelling study of the interactions between aerosols and PBL meteorology during a haze episode in  
594 China Jing-Jin-Ji and its near surrounding region - Part 2: Aerosols' radiative feedback effects, *Atmos.*  
595 *Chem. Phys.*, 15, 3277-3287, 2015b.

596 Wang, J., Wang, S., Jiang, J., Ding, A., Zheng, M., Zhao, B., Wong, D. C., Zhou, W., Zheng, G., Wang, L.,  
597 Pleim, J. E., and Hao, J.: Impact of aerosol-meteorology interactions on fine particle pollution during  
598 China's severe haze episode in January 2013, *Environ. Res. Lett.*, 9, 094002, 2014.



599 Wang, Y., Zhang, Q. Q., He, K., Zhang, Q., and Chai, L.: Sulfate-nitrate-ammonium aerosols over China:  
600 response to 2000–2015 emission changes of sulfur dioxide, nitrogen oxides, and ammonia, *Atmos.*  
601 *Chem. Phys.*, 13, 2635-2652, 2013.

602 Wang, Z., Li, J., Wang, Z., Yang, W., Tang, X., Ge, B., Yan, P., Zhu, L., Chen, X., Chen, H., Wand, W., Li,  
603 J., Liu, B., Wang, X., Wand, W., Zhao, Y., Lu, N., and Su, D.: Modeling study of regional severe hazes  
604 over mid-eastern China in January 2013 and its implications on pollution prevention and control, *Sci.*  
605 *China Earth Sci.*, 57, 3-13, 2014.

606 Xu, G., Chen, D., Xue, J., Sun, J., Shen, X., Shen, Y., Huang, L., Wu, X., Zhang, H., and Wang, S.: The  
607 program structure designing and optimizing tests of GRAPES physics, *Chinese Sci. Bull.*, 53, 3470–  
608 3476, doi:10.1007/s11434-008-0418-y, 2008.

609 Yang, Y., Liao, H., and Lou, S.: Increase in winter haze over eastern China in recent decades: Roles of  
610 variations in meteorological parameters and anthropogenic emissions, *J. Geophys. Res. Atmos.*, 121,  
611 13050-13065, 2016.

612 Yang, X., Hu, J., Chen, D., Zhang, H., Shen, X., Chen, J., and Ji, L.: Verification of GRAPES unified global  
613 and regional numerical weather prediction model dynamic core, *Chinese Sci. Bull.*, 53, 3458–3464,  
614 doi:10.1007/s11434-008-0417-z, 2008.

615 Yang, X. S., Chen, J. B., and Hu, J. L.: A semi-implicit semi-Lagran global nonhydrostatic model and the  
616 polar discretization scheme, *Sci. China Ser D-Earth Sci.*, 50, 1885-1891, 2007.

617 Yang, Y. R., Liu, X. G., Qu, Y., An, J. L., Jiang, R., Zhang, Y. H., Sun, Y. L., Wu, Z. J., Zhang, F., Xu, W. Q.,  
618 and Ma, Q. X.: Characteristics and formation mechanism of continuous hazes in China: a case study  
619 during the autumn of 2014 in the North China Plain, *Atmos. Chem. Phys.*, 15, 8165–8178,  
620 doi:10.5194/acp-158165-2015, 2015.

621 Zhang, M., Wang, H., Zhang, X., Peng, Y., and Che, H.: Applying the WRF double-moment six-class  
622 microphysics scheme in the GRAPES\_Meso model: A case study, *J. Meteor. Res.*, 32, 246, doi:  
623 10.1007/s13351018-7066-1, 2018.

624 Zhang, R., and Shen, X.: On the development of the GRAPES – a new generation of the national  
625 operational NWP system in China, *Chinese Sci. Bull.*, 53, 3429–3432, doi:10.1007/s11434008-0462-7,

626 2008.

627 Zhang, R. H., Li, Q., and Zhang, R. N.: Meteorological conditions for the persistent severe fog and haze  
628 event over eastern China in January 2013, *Sci. China Earth Sci.*, 57, 26–35, 2014.

629 Zheng, G. J., Duan, F. K., Su, H., Ma, Y. L., Cheng, Y., Zheng, B., Zhang, Q., Huang, T., Kimoto, T., Chang,  
630 D., Pöschl, U., Cheng, Y. F., and He, K. B.: Exploring the severe winter haze in Beijing: the impact of  
631 synoptic weather, regional transport and heterogeneous reactions, *Atmos. Chem. Phys.*, 15, 2969–2983,  
632 doi:10.5194/acp-15-2969-2015, 2015.

633 Zheng, G. J., Duan, F. K., Ma, Y. L., Zhang, Q., Huang, T., Kimoto, T. K., Cheng, Y. F., Su, H., and He, K. B.:  
634 Episode-based evolution pattern analysis of haze pollution: method development and results from  
635 Beijing, China, *Environ. Sci. Technol.*, 50, 4632–4641, 2016.

636 Zhong, J., Zhang, X., Dong, Y., Wang, Y., Liu, C., Wang, J., Zhang, Y., and Che, H.: Feedback effects of  
637 boundary-layer meteorological factors on cumulative explosive growth of PM<sub>2.5</sub> during winter heavy  
638 pollution episodes in Beijing from 2013 to 2016, *Atmos. Chem. Phys.*, 18, 247–258,  
639 <https://doi.org/10.5194/acp18-247-2018>, 2018a.

640 Zhong, J., Zhang, X., Wang, Y., Liu, C., and Dong, Y.: Heavy aerosol pollution episodes in winter Beijing  
641 enhanced by radiative cooling effects of aerosols, *Atmos. Res.*, 209, 59-64, 2018b.

642 Zhong, J., Zhang, X., Wang, Y., Sun, J., Zhang, Y., Wang, J., Tan, K., Shen, X., Che, H., and Zhang, L.:  
643 Relative contributions of boundary-layer meteorological factors to the explosive growth of PM<sub>2.5</sub> during  
644 the red-alert heavy pollution episodes in Beijing in December 2016, *J Meteorol. Res.*, 31, 809–819,  
645 2017.

646 Zhou, C., Gong, S., Zhang, X., Liu, H., Xue, M., Cao, G., An, X., Che, H., Zhang, Y., and Niu, T.: Towards  
647 the improvements of simulating the chemical and optical properties of Chinese aerosols using an  
648 online coupled model CUACE/Aero, *Tellus B*, 64, 18965, doi:10.3402/tellusb.v64i0.18965, 2012.

649 Zhou, C., Zhang, X., Gong, S., Wang, Y., and Xue, M.: Improving aerosol interaction with clouds and  
650 precipitation in a regional chemical weather modeling system, *Atmos. Chem. Phys.*, 16, 145-160, 2016.

651

652

653

654

Table 1. Physical and chemical processes in GRAPES\_CUACE.

Process	Option	Reference
Explicit precipitation	WDM6	Lim and Hong (2010)
Cumulus cloud	KFETA scheme	Kain (2004)
Longwave radiation	Goddard	Chou et al. (2001)
Shortwave radiation	Goddard	Chou et al. (1998)
Surface layer	SFCLAY scheme	Pleim (2007)
PBL	MRF scheme	Hong et al. (1996, 2006)
Land surface	SLAB scheme	Kusaka et al. (2001)
Gas-phase chemistry	RADM II	Stockwell et al. (1990)
Aerosol	CUACE	Zhou et al. (2012)
Aerosol direct effect	External mixing	Wang et al. (2015)
Aerosol indirect effect	CAUCE+WDM6	Zhou et al. (2016)

655

656

657

658

659

660

661

662

663

664

665

666

667

668

669

670

671

672

673

Table 2. Design of sensitivity experiments.

---

Experiment	Description
EXP1	Background experiment: ignoring aerosol radiation and conventional DC of chemical tracers by PBL scheme in GRAPES_CUACE
EXP2	Online AF online and conventional DC of chemical tracers by PBL scheme in GRAPES_CUACE
EXP3	Online AF and DC of chemical tracers set to 20% of conventional DC calculated by PBL scheme, representing compensation for the deficient description of extremely weak turbulent diffusion by the PBL scheme; DC in physical and dynamic processes the same as EXP1

---

674

675

676  
677  
678  
679  
680  
681  
682  
683  
684  
685  
686  
687  
688  
689  
690  
691  
692  
693  
694  
695  
696  
697

Table 3. VOCs in the emissions data.

VOC	Full name
ALD	Acetaldehyde and higher aldehydes
CH4	Methane
CSL	Cresol and other hydroxy substituted aromatics
ETH	Ethane
HC3	Alkanes w/ $2.7 \times 10^{-13} > \text{kOH} < 3.4 \times 10^{-12}$
HC5	Alkanes w/ $3.4 \times 10^{-12} > \text{kOH} < 6.8 \times 10^{-12}$
HC7	w/kOH $> 6.8 \times 10^{-12}$
HCHO	Formaldehyde
ISOP	Isoprene
KET	Ketones
OL2	Ethene
OLI	Internal olefins
OLT	Terminal olefins
ORA2	Acetic and higher acids
PAR	Paraffin carbon bond
TERPB	Monoterpenes
TOL	Toluene and less reactive aromatics
XYL	Xylene and more reactive aromatics

698

699

700

Table 4. Observed and modeled daily AOD (\* stands for shortage of observation).

701

702

703

704

705

706

707

708

709

710

711

Date	Shijiazhuang		Beijing		Xianghe	
	OBS	MODEL	OBS	MODEL	OBS	MODEL
15	0.46	0.55	0.07	0.12	0.10	0.15
16	0.62	0.60	0.14	0.18	0.60	0.40
17	1.30	1.10	0.50	0.56	1.33	1.05
18	1.42	1.20	0.69	0.75	0.87	0.97
19	1.26	1.30	0.50	0.86	0.96	0.90
20	*	1.20	1.90	1.70	*	1.50
21	*	0.65	1.76	1.50	1.78	1.60
22	0.18	0.30	0.10	0.20	0.18	0.22

712

713

Table 5. Observed and modeled daily SSA (\* stands for shortage of observation).

714

715

716

717

718

Date	Shijiazhuang		Beijing		Xianghe	
	OBS	MODEL	OBS	MODEL	OBS	MODEL
15	0.83	0.85	0.81	0.83	0.86	0.84
16	0.83	0.85	0.88	0.86	0.92	0.86
17	0.88	0.89	0.88	0.90	0.93	0.90
18	0.87	0.89	0.91	0.92	0.90	0.90
19	0.86	0.91	0.90	0.93	0.92	0.91
20	*	0.90	*	0.93	*	0.92
21	*	0.88	0.93	0.93	*	0.90
22	0.82	0.83	0.84	0.86	0.88	0.84

719

720

### Figure captions

721 **Fig. 1.** (a) Model domain and location of Jing–Jin–Ji. (b) Geographic location and topography of Jing–Jin–  
722 Ji. Blue dots are the locations of PM<sub>2.5</sub> observations; red triangles are the locations of automatic weather  
723 stations; yellow stars are the two sounding stations; black crosses are the CARSNET and AEROSNET  
724 stations.

725 **Fig. 2.** Geopotential height (color-shaded; gp10m), temperature (dashed black contours; K) and wind (wind  
726 bars; m/s) in the (a) upper (500 hPa) and (b) middle (700 hPa) atmosphere, and geopotential height and  
727 wind in the (c) lower atmosphere (850 hPa) and (d–f) PBL (900, 950, 1000 hPa), at 0000 UTC 19  
728 December 2016.

729 **Fig. 3.** Observed and modeled wind speed and temperature at the surface (upper panels), and the PBL-mean  
730 wind speed and temperature (lower panels), from the results of EXP1, EXP2 and EXP3 for Beijing, Xingtai,  
731 and the average for Jing–Jin–Ji as a whole, during 15–24 December 2016.

732 **Fig. 4.** Mean observed (OBS\_PM<sub>2.5</sub>) and modeled PM<sub>2.5</sub> concentration ( $\mu\text{g}/\text{m}^3$ ) of the PM<sub>2.5</sub> explosive  
733 growth stage, from the results of EXP1, EXP2 and EXP3 (PM<sub>2.5</sub>\_EXP1, PM<sub>2.5</sub>\_EXP2 and PM<sub>2.5</sub>\_EXP3,  
734 respectively).

735 **Fig. 5.** Mean percentage change in SDSRF ( $\text{W}/\text{m}^2$ ) owing to (a) aerosols and (b) aerosols+DTD during the  
736 explosive growth stage.

737 **Fig. 6.** Profiles of average temperature change in Jing–Jin–Ji owing to AF (K) during 15–20 December  
738 2016.

739 **Fig. 7.** Sounding-observed and modeled temperature profiles in EXP1 and EXP2 during the (a) climbing  
740 stage and (b) explosive growth stage in Beijing and Xingtai.

741 **Fig. 8.** Hourly change of PM<sub>2.5</sub>\_OBS, PM<sub>2.5</sub>\_EXP1, PM<sub>2.5</sub>\_EXP2, and PM<sub>2.5</sub>\_EXP3 ( $\mu\text{g}/\text{m}^3$ ), together with  
742 the DC at 950 hPa of the three experiments (DC\_EXP1, DC\_EXP2, DC\_EXP3) during 15–22 December  
743 2016 in (a) Beijing and (b) Xingtai.

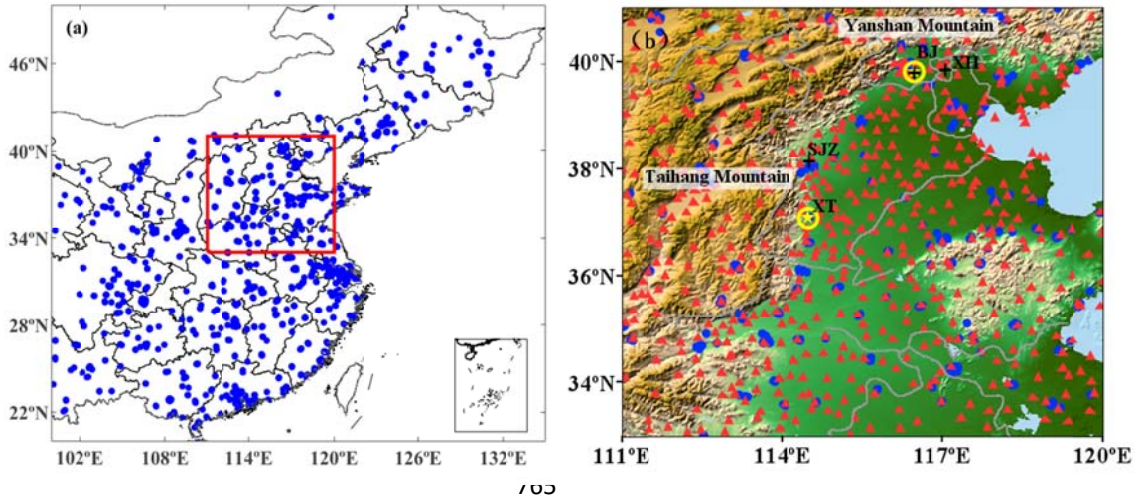
744 **Fig. 9.** Diagrammatic sketch of the contributions of AF and DTD to the PM<sub>2.5</sub> explosive growth.

745

746

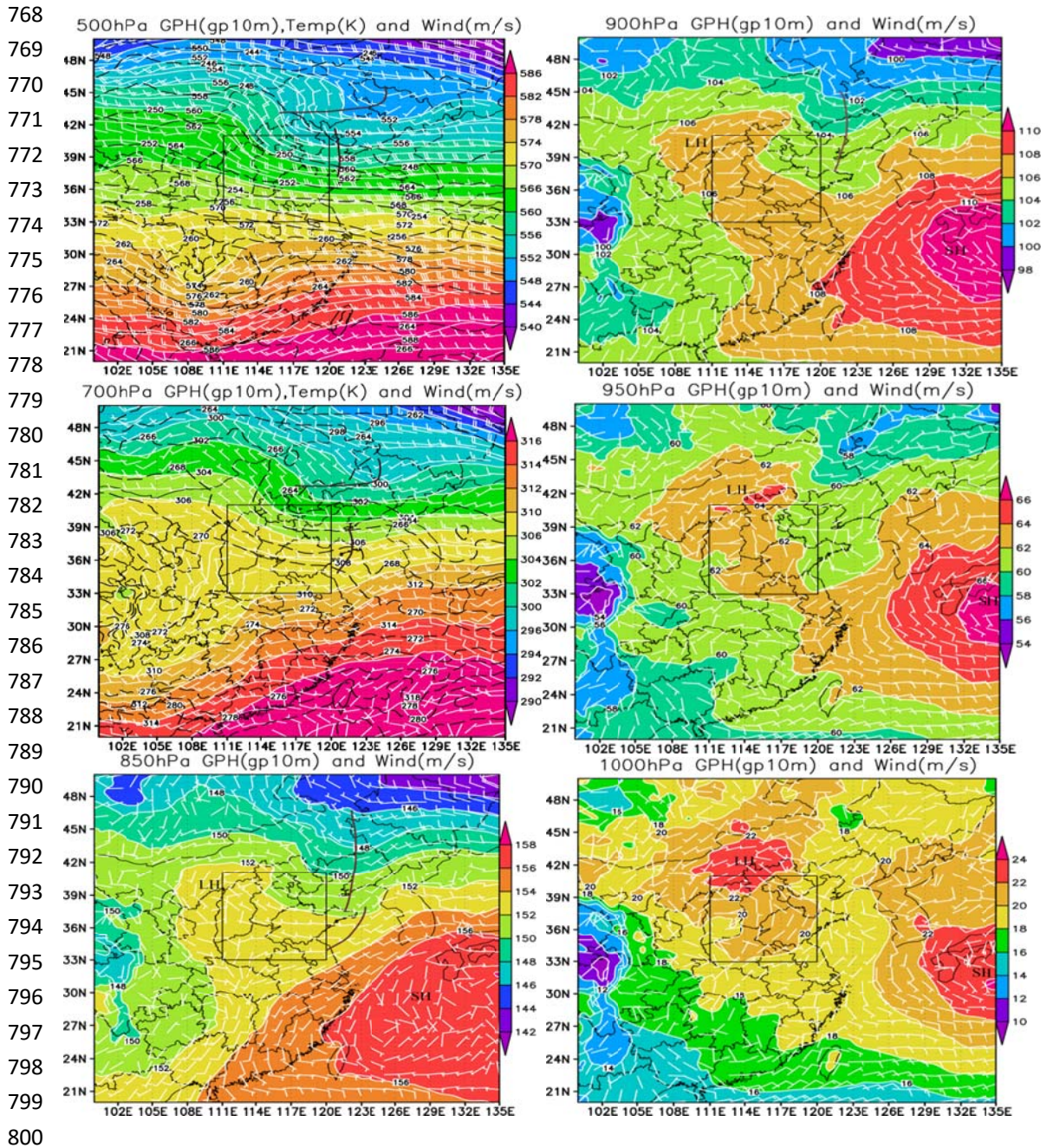
747

749  
750  
751  
752



765 **Fig. 1.** (a) Model domain and location of Jing–Jin–Ji. (b) Geographic location and topography of Jing–Jin–  
766 Ji. Blue dots are the locations of PM<sub>2.5</sub> observations; red triangles are the locations of automatic weather  
767 stations; yellow stars are the two sounding stations; black crosses are the CARSNET and AEROSNET  
768 stations.  
766  
767





804 **Fig. 2.** Geopotential height (color-shaded; gp10m), temperature (dashed black contours; K) and wind (wind  
805 bars; m/s) in the (a) upper (500 hPa) and (b) middle (700 hPa) atmosphere, and geopotential height and  
806 wind in the (c) lower atmosphere (850 hPa) and (d-f) PBL (900, 950, 1000 hPa), at 0000 UTC 19  
807 December 2016.

805

806

806  
807  
808  
809  
810  
811  
812  
813  
814  
815  
816  
817  
818  
819  
820  
821  
822  
823  
824  
825  
826  
827  
828  
829  
830  
831  
832  
833  
834  
835  
836  
837  
838  
839  
840  
841  
842  
843  
844  
845

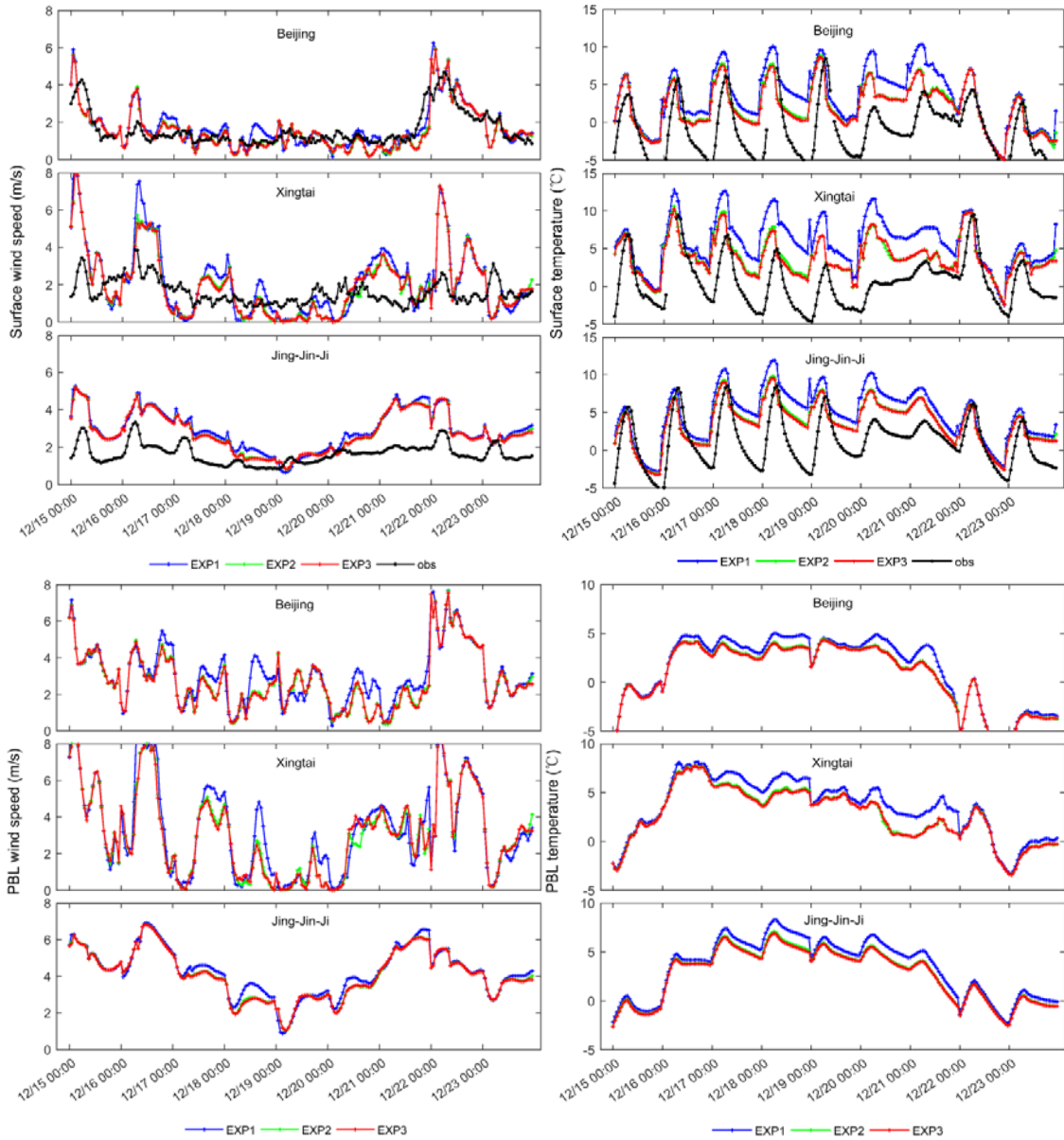


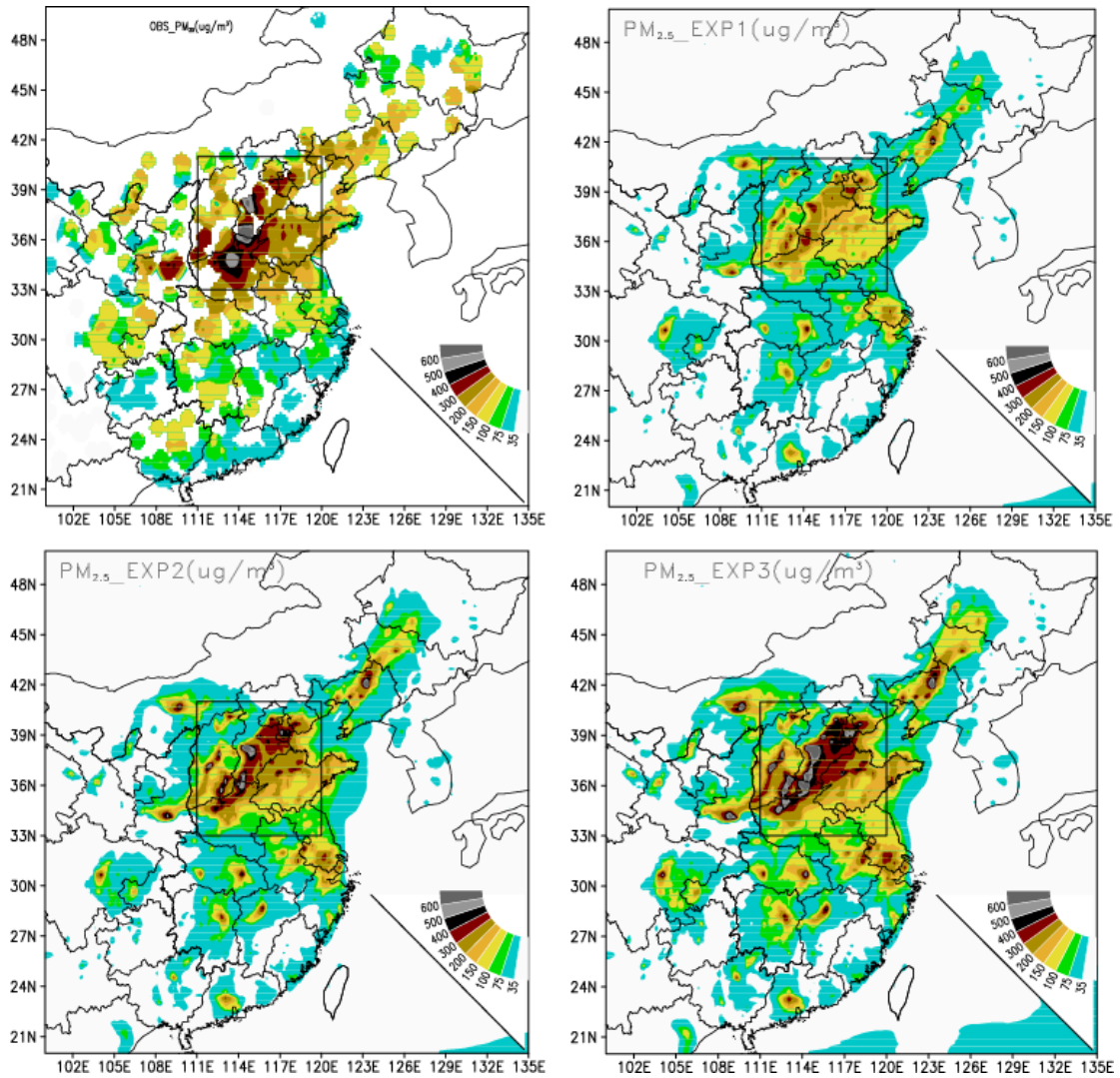
**Fig. 3.** Observed and modeled wind speed and temperature at the surface (upper panels), and the PBL-mean wind speed and temperature (lower panels), from the results of EXP1, EXP2 and EXP3 for Beijing, Xingtai, and the average for Jing–Jin–Ji as a whole, during 15–24 December 2016.



846

847

848



849

850

851 **Fig. 4.** Mean observed (OBS\_PM<sub>2.5</sub>) and modeled PM<sub>2.5</sub> concentration ( $\mu\text{g}/\text{m}^3$ ) of the PM<sub>2.5</sub> explosive

852 growth stage, from the results of EXP1, EXP2 and EXP3 (PM<sub>2.5</sub>\_EXP1, PM<sub>2.5</sub>\_EXP2 and PM<sub>2.5</sub>\_EXP3,

853 respectively).

854

855

856

857

858

860  
861  
862  
863  
864  
865  
866  
867  
868  
869  
870  
871  
872  
873  
874  
875  
876  
878  
879  
880  
881  
882

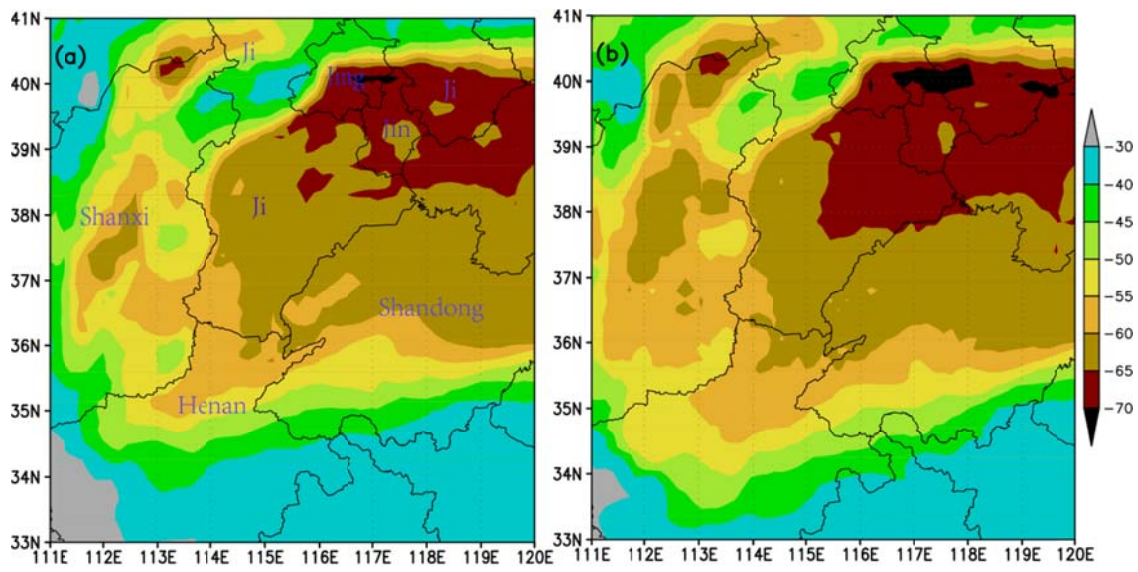


**Fig. 5.** Mean percentage change in SDSRF ( $W/m^2$ ) owing to (a) aerosols and (b) aerosols+DTD during the explosive growth stage.

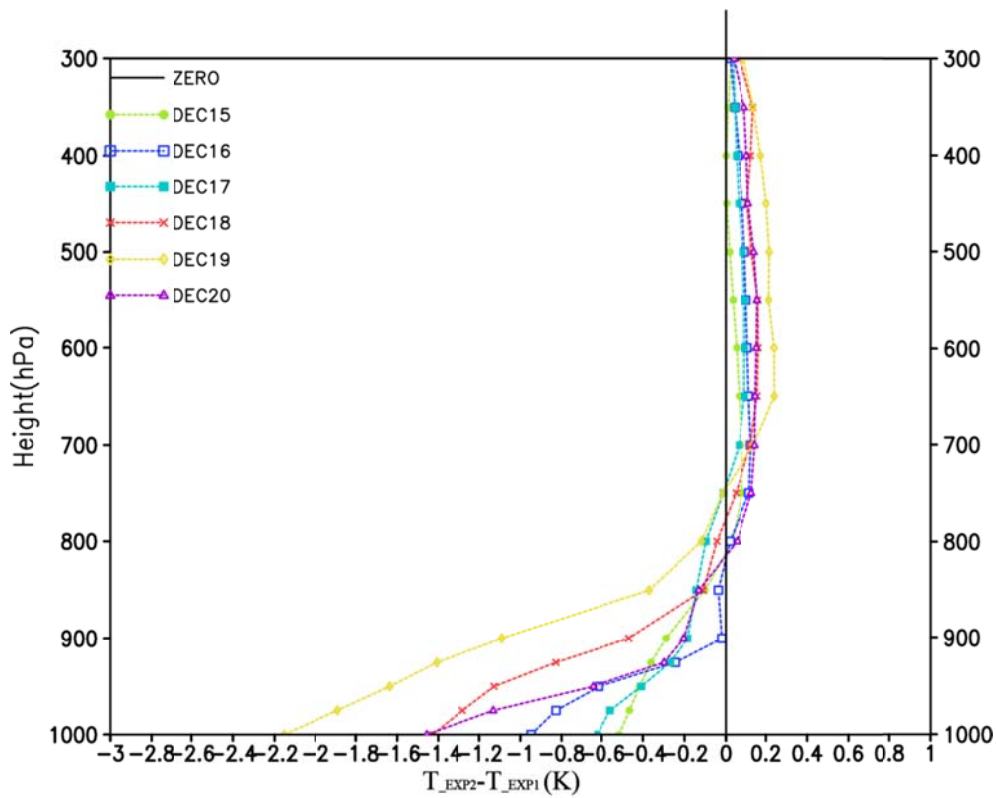
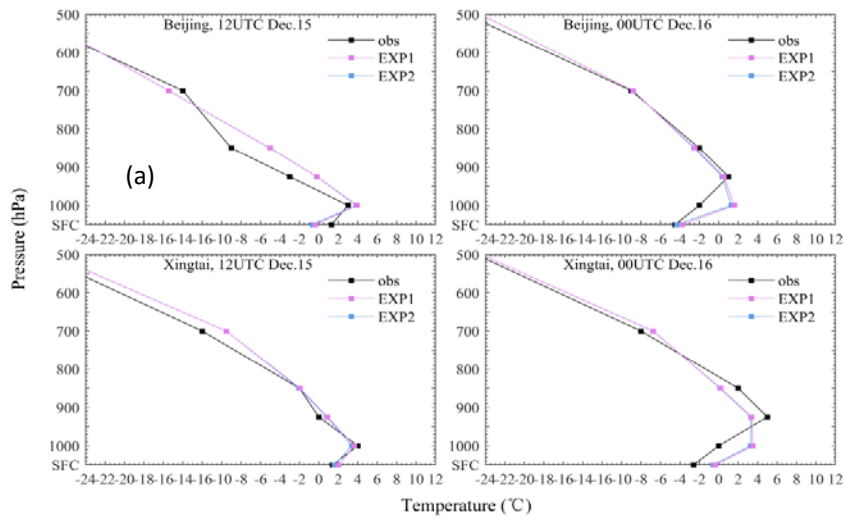
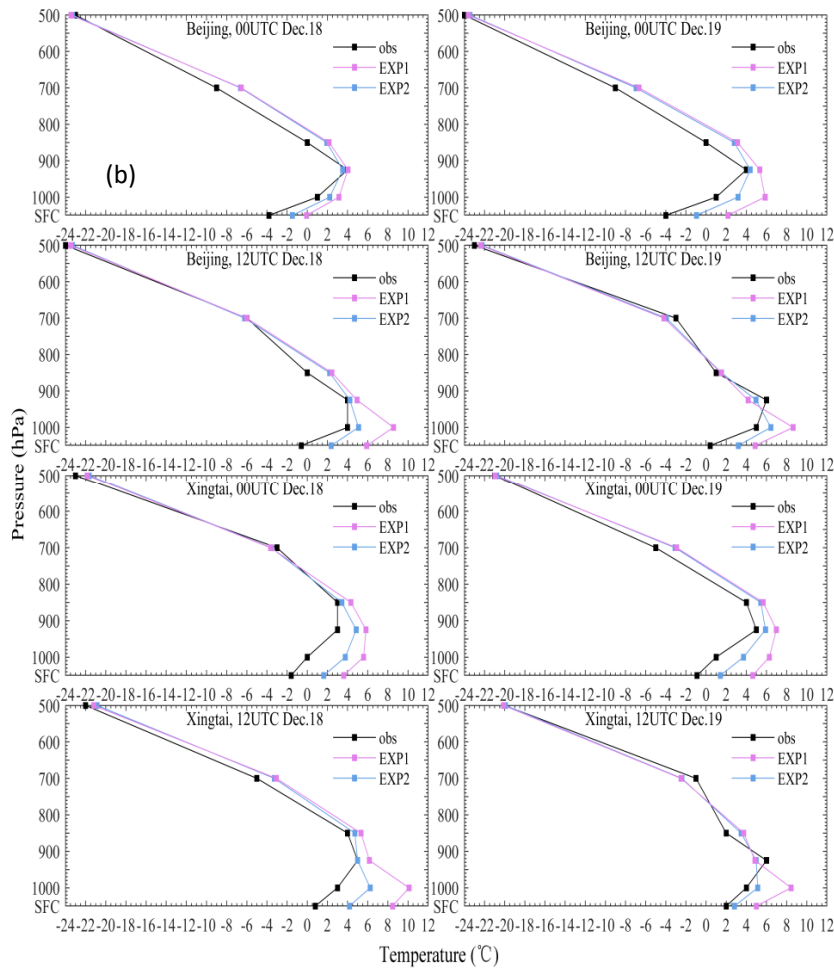


Fig. 6. Profiles of average temperature change in Jing-Jin-Ji owing to AF (K) during 15–20 December 2016.



920

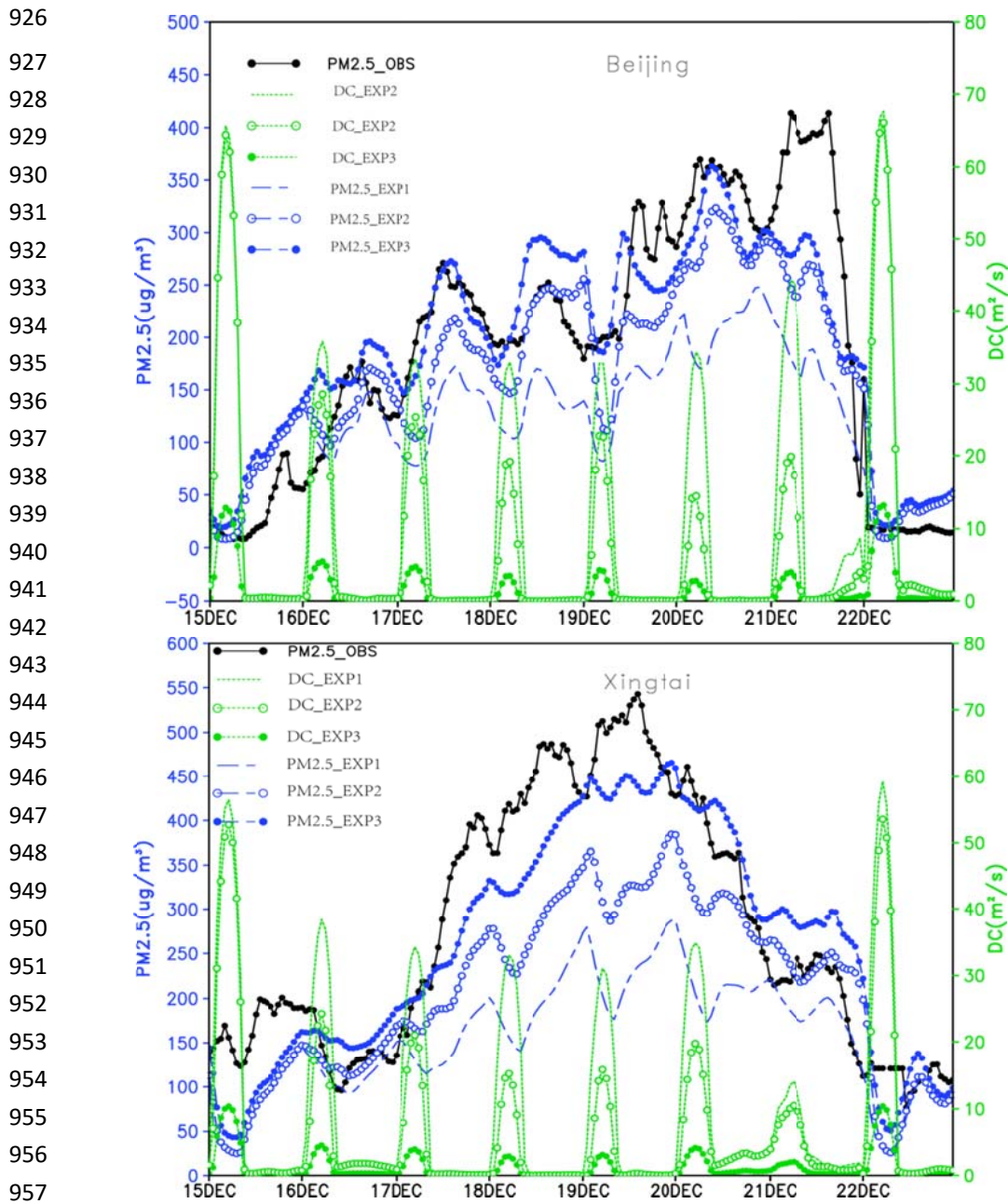


921

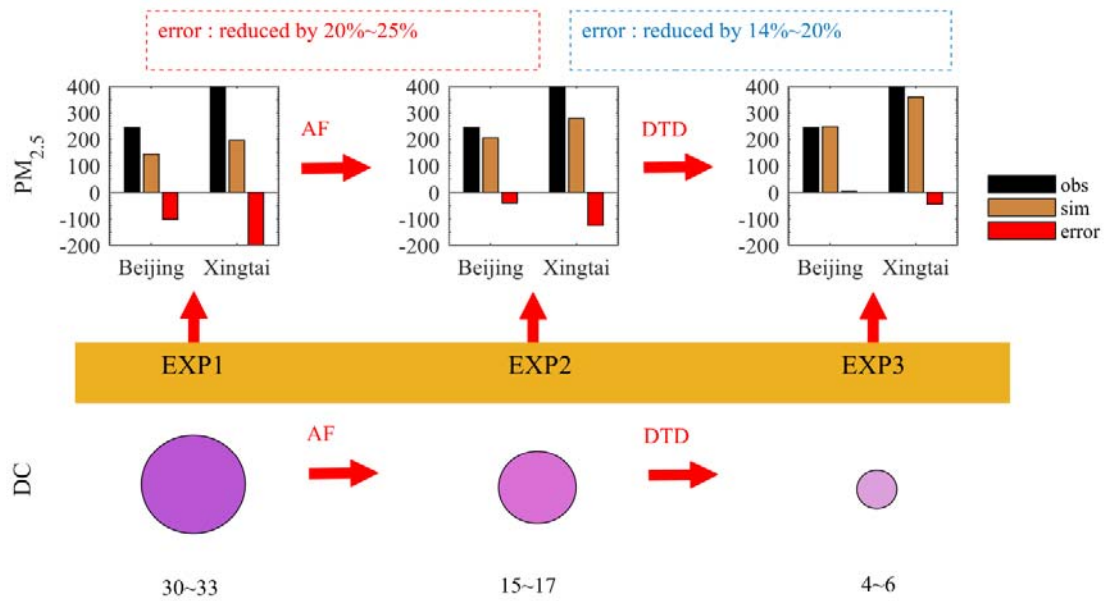
922 **Fig. 7.** Sounding-observed and modeled temperature profiles in EXP1 and EXP2 during the (a) climbing

923 stage and (b) explosive growth stage in Beijing and Xingtai.

924



926  
 927  
 928  
 929  
 930  
 931  
 932  
 933  
 934  
 935  
 936  
 937  
 938  
 939  
 940  
 941  
 942  
 943  
 944  
 945  
 946  
 947  
 948  
 949  
 950  
 951  
 952  
 953  
 954  
 955  
 956  
 957  
 960 **Fig. 8.** Hourly change of PM<sub>2.5</sub>\_OBS, PM<sub>2.5</sub>\_EXP1, PM<sub>2.5</sub>\_EXP2, and PM<sub>2.5</sub>\_EXP3 ( $\mu\text{g}/\text{m}^3$ ), together with  
 961 the DC at 950 hPa of the three experiments (DC\_EXP1, DC\_EXP2, DC\_EXP3) during 15–22 December  
 962 2016 in (a) Beijing and (b) Xingtai.



960  
 961  
 962  
 963  
 964  
 965

**Fig. 9.** Diagrammatic sketch of the contributions of AF and DTD to the PM<sub>2.5</sub> explosive growth.